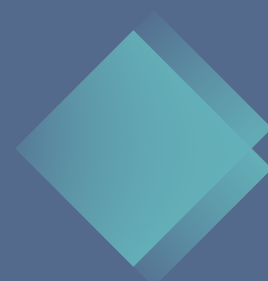


Krzysztof Strzecha

**Selected Algorithms
of Quantitative Image
Analysis for Measurements
of Properties Characterizing
Interfacial Interactions
at High Temperatures**

**Monographs 2016
Lodz University of Technology**



Krzysztof Strzecha

**Selected Algorithms
of Quantitative Image
Analysis for Measurements
of Properties Characterizing
Interfacial Interactions
at High Temperatures**

**Monographs 2016
Lodz University of Technology**

Reviewed by:
Professor Dominik Sankowski
Professor Kazimierz Wiatr

Scientific Editor
Faculty of Electrical, Electronic, Computer and Control Engineering
Professor Piotr Ostalczyk

© Faculty of Electrical, Electronic,
Computer and Control Engineering 2016

LODZ UNIVERSITY OF TECHNOLOGY PRESS

90-924 Lodz, 223 Wolczanska Street
phone/42 631-20-87, 42 631 29 52,
fax 42 631-25-38

e-mail: zamowienia@info.p.lodz.pl
www.wydawnictwa.p.lodz.pl

ISBN 978-83-7283-742-4

Edition 100 copies
Printed by
Offset printing „Quick-Druk” s.c. 90-562 Lodz, 11 Łąkowa Street
No. 2168

Contents

1. Introduction	4
2. Measurements of the Surface Tension and Contact Angle	8
2.1. Review of Selected Solutions.....	9
2.2. Sessile Drop Method.....	10
3. THERMO-WET Measurement System	14
3.1. Construction of the Measurement System	15
3.2. Software of the Measurement System	16
3.2.1. Project Specification.....	17
3.2.2. Modular Structure.....	18
3.2.3. Serial Communication	19
3.2.4. Task Experiment Scheduler Module.....	23
4. Image Enhancement.....	25
4.1. Removal of Instrumental Background	26
4.2. Compensation of Pixel Non-uniform Response	28
4.3. Automatic Change of Optical Filters.....	29
4.4. Switching Median Filter.....	35
5. Correction of the Image Distortions Influenced by the Gas Flow.....	46
5.1. Correction of the “Gas lens” Effects.....	49
5.2. Aura Removal.....	54
6. Segmentation	57
6.1. Algorithm for Fast Specimen Localization	57
6.2. Edge Detection with Dynamic Selection of Filtration Masks.....	59
6.3. Contour Tracing.....	61
6.4. Profile Correction at the Contact Point of the Three Phases	62
6.5. Subpixel Edge Detection.....	66
7. Conclusions.....	72
Bibliography	75

1. Introduction

In the case of every quantitative image analysis system a very important issue is to improve the quality of images to be analyzed, in other words, their pre-processing. As a result of pre-processing, the significant part of the redundant information and disturbances (which could originate from imperfect vision system components) should be removed from the image.

Another particularly important problem to be solved is the right choice of image segmentation procedures. Segmentation essence is to divide an image into disjoint subsets that meet certain criteria for homogeneity (e.g. color, brightness or texture). The result of segmentation should allow the most precise determination of geometrical features of objects present in a scene with a minimum of computing effort. The measurement of geometric properties of objects present in the scene is the subject of image analysis.

In the rich literature on the subject many pre-processing algorithms have been presented (Ballard and Brown, 1982; Gonzalez and Wintz, 1987; Pavlidis, 1987; Jain, 1989; Lim, 1990; Materka, 1991; Chellappa, 1992; Shapiro and Rosenfeld, 1992; Dougherty and Astola, 1993; Teuber, 1993; Baxes, 1994; Dougherty, 1994; Awcock and Thomas, 1995; Watkins et al., 1995; Castleman, 1996; Woźnicki, 1996; Tadeusiewicz and Korohoda, 1997; Bovik, 2000; Erhardt-Ferron, 2000; Hader, 2000; Shapiro and Stockman, 2000; Zuech, 2000; Nikolaidis and Pitas, 2001; Pitas, 2001; Jahne, 2002; Russ, 2002; Sharma, 2002; Wiatr, 2002, Forsyth and Ponce, 2003; Wiatr, 2003; Davies, 2004; Jahne, 2004; Jensen, 2004; Acharya and Ajoy, 2005; Umbaugh, 2005; Bauer, 2006; Woods, 2006; Gonzalez and Woods, 2007; Pratt, 2007; Sonka et al., 2007; Sankowski et al., 2011; Tadeusiewicz i Śmietański, 2011). Unfortunately, their usage often results in a loss of image information which may be important for the purpose of analysis. In most systems of the quantitative analysis of images, the accuracy of the object shape and dimension determination is critical for the measurement process, so it is advisable to develop quality improvement algorithms which does not cause loss of information on the exact location of the edges.

Despite significant progress in the field of image processing and analysis, the problem of the development of pre-processing algorithms that do not cause significant loss of image information is still not resolved. This is due to

the fact that most of the known processing algorithms for improving the image quality do not consider information on the properties of vision systems by means of which processed images were obtained.

Literature on the subject also describes a number of algorithms for image segmentation (Fu et al., 1981; Haralick and Shapiro, 1985; Reed and du Buf, 1993; Tadeusiewicz and Korohoda, 1997; Li and Gray, 2000; Suri et al., 2002; Yoo, 2004; Nieniewski, 2005; Suri et al., 2005; Sun, 2006; Zhang, 2006; Sankowski et al., 2011, Tadeusiewicz i Śmietański, 2011). In all cases, existing mathematical algorithms need to be supported by heuristic solutions and a priori knowledge about the processed image. It does not seem possible to eliminate these two factors. It is appropriate, however, to search for algorithms which, on one hand, use them minimally, while on the other, do not require modification when they change. Such algorithms could be applied to a broad class of images in a very large range of applications.

The problem of developing algorithms for image segmentation which work for a wide class of images is still far from a satisfactory solution. It is necessary to search for new methods which will provide high-quality processing with the minimal use of a priori knowledge of the scene analyzed. Thus, they may be used in a wide range of applications of quantitative image analysis systems.

Among the methods of image analysis, a special place is occupied by algorithms of the precise edge localization with the sub-pixel accuracy. Issues related to the use of these methods for industrial application qualitative image analysis have not yet been fully identified or studied.

The main aim of the research described in this book was to develop, implement and verify the modern methods of image processing and analysis which could successfully be used in industrial quantitative image analysis systems.

All the algorithms described in the book have been implemented and tested on a THERMO-WET measurement stand. The THERMO-WET is a computerized device for the automated measurement of surface phenomena occurring during contact of liquid and solid phases. It is capable of measuring the surface tension of a liquid (surface energy) and the wetting angle of a solid by a liquid (including an extreme wetting angle). These parameters are determined using the sessile drop method. These tests can be conducted

in a controlled atmosphere, in a temperature range of up to 1800°C, for interfacial solid-liquid systems of two different materials.

The algorithms developed and presented in the book include:

- **Image quality improvement** – the accuracy of measurement is highly influenced by errors contributed by all the elements of a vision system. This problem can be solved through the development of specialized algorithms for the compensation of the negative impact of the vision system components.
- **Correction of errors contributed to an image by the flow of protective gas** – a gas flow at high temperatures causes a number of phenomena affecting the exact localization of the specimen edges, especially "gas lens" and "aura". An attempt was made to solve this problem by creating specialized algorithms for the compensation of the impact of these phenomena.
- **Image segmentation** – the quality of segmentation has a critical impact on the accuracy of the measurement of geometric parameters. The specificity of images taken at high temperatures makes the segmentation process particularly difficult and requires the use of specialized, dedicated algorithms. The algorithms developed are designed to improve the quality of segmentation, and thus allow the accurate representation of the edge of the sample in the resulting image, in particular in the area of contact points of the three phases.

This book is divided into seven chapters. Chapter 1 provides a brief introduction to the content of the book and Chapter 7 is its brief summary. The main content of the book is contained in Chapters 2 to 6.

The second chapter presents the problem of the surface tension and contact angle measurements. The review of selected solutions is included. The sessile drop method is described in detail.

Chapter 3 presents the THERMO-WET measurement system. Its design, with a particular emphasis on software is discussed.

In Chapter 4 image enhancement algorithms are described. Their main goal is to compensate the negative impact of the components of a vision system. The following algorithms are presented and discussed in detail: the removal of an instrumental background, the compensation of a pixel non-uniform response, the automatic change of optical filters and a switching median filter.

Algorithms for the correction of the image distortions influenced by the protective gas flow are presented in Chapter 5. They include the correction of the “gas lens” effects and aura removal methods.

Chapter 6 is devoted to the specialized segmentation algorithms, developed specially for the THERMO-WET system. The following algorithms are presented: the fast specimen localization, edge detection with dynamic selection of filtration masks, contour tracing, profile correction at the contact point of the three phases, subpixel edge detection.

2. Measurements of the Surface Tension and Contact Angle

In many industrial processes, an important and sometimes a predominant role is played by the phenomena occurring at the interfaces of the liquid, the gas and the solid state. These phenomena occur in welding, the making of composite materials with the participation of the liquid phase, the sintering of powders, the saturation of porous structures, coating, the refining of metals to eliminate non-metallic inclusions, foundry or processes of crystallization from the liquid phase. Thus, the knowledge of physical-chemical processes occurring between the liquid, the gas and the solid is a significant technological problem.

A number of monographs and review articles have been devoted to the significance of phenomena at the interfaces in different fields of technology: (Metcalfe, 1981; Pask and Evans, 1981; Matsunawa and Ohji, 1982; Matsunawa and Ohji, 1983; Matsunawa and Ohji, 1984; Delannay et al., 1987; Baglin, 1988; Nicholas, 1990; Senkara and Windyga, 1990; Mortensen, 1991; Eustathopoulos et al., 1999; Drzymała, 2001; Butt et al., 2003; de Gennes et al., 2003; Popel, 2003; Rosen, 2004; Deyev and Deyev, 2005; Venables, 2006; Trakhtenberg et al., 2007; Bracco and Holst, 2013). Theoretical foundations of surface phenomena physics and methods of measurement can be found in books: (Woodruff, 1973; Missol, 1974; Murr, 1975; Zangwill, 1988; Adamson and Gast, 1997; Dutkiewicz, 1998; Myers, 1999; Safran, 2003; Hartland, 2004; Bechstedt, 2005; Woodruff, 1996; Mittal, 2006; Ibach, 2007; Bracco and Holst, 2013), and review papers (Kinloch, 1980; de Gennes, 1985; Kwok and Neumann, 2000; Lam et al., 2001a; Lam et al., 2001b; Xu and Masliyah, 2002; Cwikel et al., 2010).

Among the basic measurable quantities characterizing surface interactions are the surface energy (surface tension) of the liquid phase and the extreme angle of wetting of the base by a liquid. Measurements and calculations performed for the conditions of the thermodynamic equilibrium. For many systems, however, this equilibrium is not reached at all or is reached after too long a time from the technological point of view. This results from processes of diffusion, the dissolution of the base in the liquid, the formation of new chemical compounds or inter-metallic phases. In such cases, crucial information is obtained by measuring dynamic, time-variable quantities of the system,

possibly in combination with a structural analysis of the interfacial boundary carried out later.

The investigation of the interfacial processes occurring in the solid-liquid or liquid-liquid systems of two different materials is associated with a number of difficulties, resulting, among others, from the activity of the materials in the liquid state, the need for a precisely controlled atmosphere composition, the sensitivity to contamination, carrying out measurements at high and even very high temperatures which must be controlled with high precision. In many cases, it is necessary to track changes of interfacial processes in transient states (e.g. in the steel metallurgy at the interface of the molten metal and slag substances).

2.1. Review of Selected Solutions

For a long time, the optical methods, based on the continuous observation of the specimen (or droplet) shape and the manual or photographic recording of changes in its profile as a function of temperature, were the fundamental techniques of determination of the wetting angle and surface tension. The profiles recorded were then analyzed by a qualified specialist who, using graphical methods, measured the basic parameters of the droplet and then calculated the values of the parameters measured. Measuring systems of this type had a number of drawbacks, only to mention an extremely labor-consuming and strenuous measurement calling for the operator's constant undivided attention, as well as an essential effect of the human factor on the measurement results.

In recent years there has been considerable progress in automated techniques for measuring the basic parameters characterizing the interfacial interactions. There are several devices on the market which allow measurement of the extreme wetting angle and the surface tension in systems of liquid metals and solids in protective atmospheres. Primarily, the PR-25/37/45 series of devices produced by the Institute for Tele- and Radio in Warsaw should be mentioned here. These devices are designed for the automatic determination of phase transition temperatures of solids (sintering, softening, melting, melts), as well as for the determination of the wetting angle and surface

tension of the melted material as a function of temperature in the range from 700°C to 1750°C.

Systems enabling fully automated measurement typically only allow the measurement of properties of selected materials in a narrow temperature range. Additionally, image processing and analysis algorithms implemented in them are not immune to interferences and require the precise positioning of the specimen (Huh and Reed, 1983; Rotenberg et al., 1983; Girault et al., 1984; Anastasiadis et al., 1987; Cheng et al., 1990; Pallas and Harrison, 1990; Hansen and Rodsrud, 1991; Egry et al. 1992; Hansen, 1993; Bachevsky et al., 1994; Song and Springer, 1996; Kernco Instruments, 1999; Atae-Allah et al., 2001; Emelyanenko and Boinovich, 2001; Emelyanenko, 2004; Zuo et al., 2007; Staldera et al., 2010).

The author was involved in the research projects 8 T10C 005 14 and N N519 403037, within the framework of which an automatic device for the measurement of the extreme angle and surface tension in systems of liquid metal and solids was developed. This device, as the first in the world, enabled automated measurement in a wide range of temperatures in a protective atmosphere (Sankowski et al., 2001a; Sankowski et al., 2011). These measurements are based on algorithms for image processing and analysis, and are conducted using the sessile drop technique.

2.2. Sessile Drop Method

The shape of the drops placed on a non-wettable surface results from two types of forces: the surface tension, which tries to give a droplet a spherical shape, and the gravity by which the drop is "flattened". In the case of the spherical drops, it is not possible to determine the surface tension. This becomes possible only when the effects of gravity are comparable with the influence of surface energy, and hence the larger droplets – the equatorial diameter of the metal droplets should be practically at least 0.5 cm. The distortion occurring in a spherical droplet allows one to determine the surface tension on the basis of the droplet dimensions and physical constants. Only symmetric drops could be taken into account (Missol, 1974).

Among the currently used methods for calculating the surface tension three groups can be distinguished:

- the method of the equatorial plane (measured h and d – Fig. 2.1);
- the method of tangents (measured Z and d);
- the method of the total height (measured z_o or z') and the maximum diameter and the diameter of the base (respectively– x_o or x') (Missol, 1974).

The determination of the equatorial plane, according to the literature, is usually performed graphically. After the measurement of h and d , the ratio of $d/2h$ is calculated. This ratio is essential for further calculations. These can be performed using Porter's formula (2.1) or using Koszewnik's tables (Missol, 1974).

$$\frac{\alpha^2}{r^2} = \left(\frac{h}{r}\right)^2 - 0,660 \left(\frac{h}{r}\right)^3 \left[1 - 4,05 \left(\frac{h}{r}\right)^2\right]; \quad (2.1)$$

where:

α – the capillary constant.

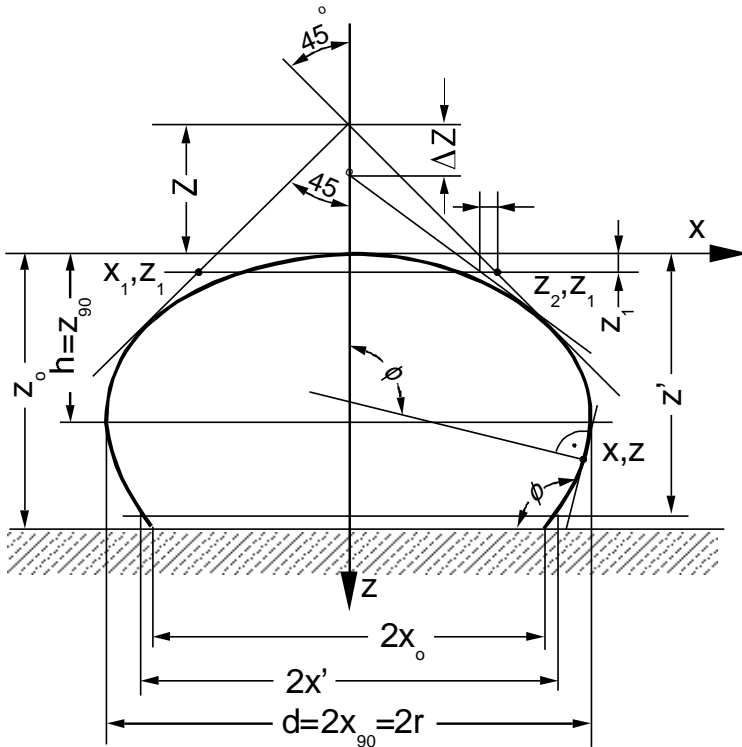


Fig. 2.1. Sessile drop (measured parameters indicated)

According to the literature, Porter equation is affected by calculation inaccuracy of several percent. For values of $d / 2h$ from 2.18 to infinity, it is valid with calculation error no more than 0.2%. Allowing the measurement error 1%, the application of this equation can be extended to the range of $d / 2h$ from 1.66 to infinity.

Dorsey, on the basis of Bashforth and Adams tables, empirically developed the following calculation formula:

$$\frac{\alpha^2}{r^2} = \frac{0,10400}{\frac{y}{r} - 0,41421} - 0,24536 + 0,0962 \left(\frac{y}{r} - 0,41421 \right); \quad (2.2)$$

which ensures the accuracy of the calculations of about 0.19% in the range of Z / r from 0.515 to 0.66 ($d / 2h$ from 1.36 to 2.18) (Missol, 1974).

The determined values of the height and the radius of the droplet allow the determination of a capillary constant. Taking into account the density of the test material, and the gravitational acceleration constant capillary, the surface tension is calculated based on the expression:

$$\sigma = g \Delta \rho \alpha^2; \quad (2.3)$$

where:

$\Delta \rho$ – the density difference, in the case of metal and the gaseous phase:

$\Delta \rho = \rho_S$, wherein ρ_S is the density of the metal;

g – the gravitational acceleration.

The determination of the contact angle is a direct measuring method on the basis of the point of contact of the three phases, in accordance with the definitional equation of Young (Fig. 2.2):

$$\left| \overline{\sigma}_{LV} \right| \cos \theta + \left| \overline{\sigma}_{SL} \right| - \left| \overline{\sigma}_{SV} \right| = 0; \quad (2.4)$$

where:

θ – the wetting angle;

$\overline{\sigma}_{SV}$ – the surface tension on the border of solid-gas;

$\overline{\sigma}_{SL}$ – the surface tension on the border of solid-liquid;

$\overline{\sigma}_{LV}$ – the surface tension on the border of liquid-gas.

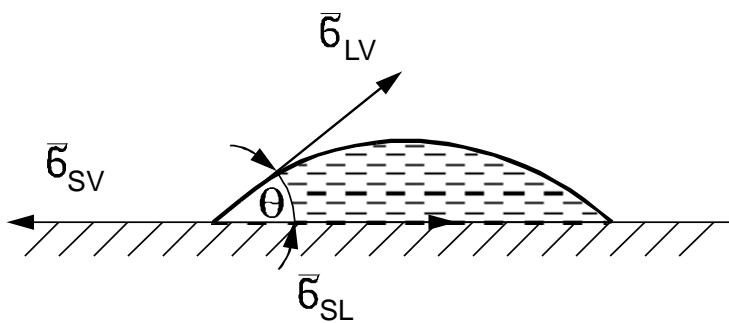


Fig. 2.2. The conditions of the thermodynamic equilibrium

3. THERMO-WET Measurement System

Within the framework of the research no. 8T10C 005 14 sponsored by the Polish National Research Committee, carried out from February 1998 until June 2000, The Computer Engineering Department of the Lodz University of Technology in co-operation of the Warsaw University of Technology and the Industrial Electronic Institute (PIE) in Warsaw built a computerized device for the automated measurement of surface phenomena occurring in contact of liquid and solid phases (Sankowski et al., 1999; Sankowski et al., 2000a; Sankowski et al., 2000b; Sankowski et al., 2001a; Sankowski et al., 2001b; Strzecha, 2002; Jeżewski, 2006; Sankowski et al., 2011). The further development of the system was conducted under the project no. N N519 403037 sponsored by Ministry of Science and Higher Education, carried out from October 2009 until October 2011 (Strzecha et al., 2010). The author was the supervisor of this project.

The developed system was named THERMO-WET. The system is capable of measuring:

- the surface tension of a liquid (surface energy);
- the wetting angle of a solid by a liquid (including extreme wetting angle).

These parameters are determined using the sessile drop method in the conditions of thermodynamic equilibrium, and in the case of transient states as a function of time and temperature. These tests may be conducted in a controlled atmosphere, in a temperature range of up to 1800°C, for interfacial solid-liquid systems of two different materials. The measurement process takes place on the basis of specialized, designed specifically for THERMO-WET system algorithms of image processing and analysis. The images processed and analyzed are obtained from a camera observing a sample of the test material placed inside the high-temperature furnace. The measurement results obtained using the presented system are characterized by a much higher accuracy and higher reproducibility compared with those obtained with the previously used, time-consuming methods, depending on the operator's subjective assessments.

3.1. Construction of the Measurement System

The measurement system consists of a two-zone high-temperature electric furnace (1) equipped with a high-precision temperature controller (2), the process gases supply system (3), the system for loading and discharge of the specimen (4), the CCD camera (5) coupled with the computer controlling the measurement process (6), equipped with a specialized programs to image process and analysis, mathematical data processing, editing and archiving of results. A general view of the system THERMO-WET is shown the photograph in Fig. 3.1. A block diagram of the system is presented in Fig. 3.2.



Fig. 3.1. The main view of computerized device for the automated measurement of the surface tension and the wetting angle

- 1 – the heating chamber of the furnace; 2 – the temperature controllers;
- 3 – the system of technological gas supply; 4 – the specimen insertion mechanism;
- 5 – the vision subsystem including CCD camera and infrared filters changer;
- 6 – the computer controlling measurement process and processing measurement data

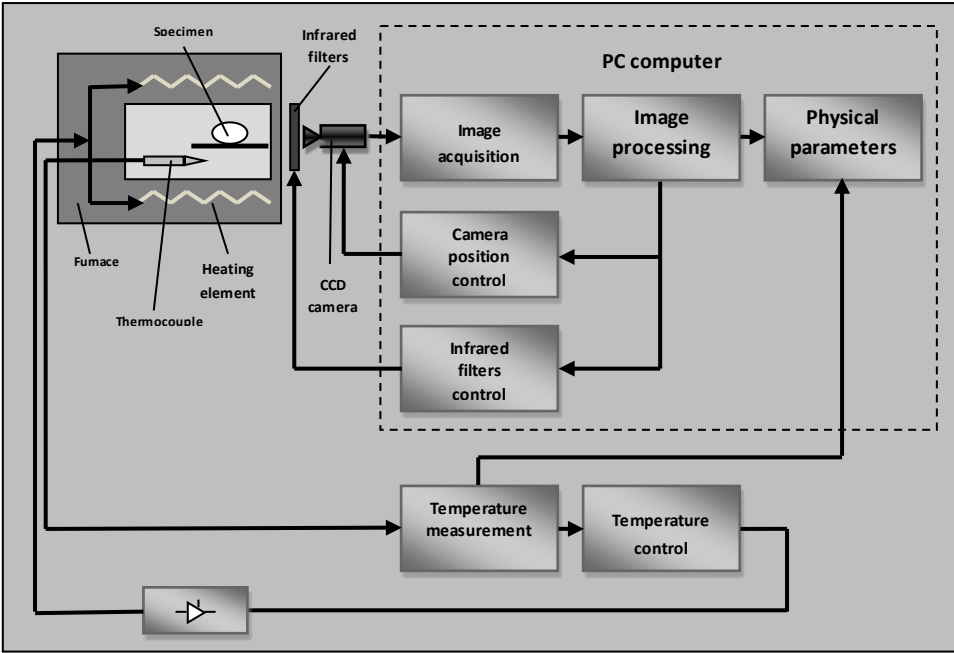


Fig. 3.2. Block diagram of the automated measurement system

3.2. Software of the Measurement System

The computer in the THERMO-WET system has a dual role: it controls the automatics of the entire device (temperature controllers, infrared filters changer) and is also the center of visual information processing. The software of the device was entirely written in C++ and is designed to run under Microsoft Windows XP (or newer) operating system.

The software can be divided into following functional blocks:

- Planning and control of the experiment. This block allows the operator to enter the following data describing the experiment: the type of a protective atmosphere, the specimen and the surface materials, the start and the end temperatures of the experiment, the rate of a temperature rise, the specimen weight and the protective atmosphere density. This block is also responsible for the control of the entire measurement process.
- Temperature measurement and control. Communication with the temperature controller takes place via the serial port using the standard MODBUS protocol. The following settings are possible: the temperature of the heating element, the power limit, the PID controller settings, the control period.

The block also allows receiving the following information sent by controllers: the temperature of the heating element, the batch temperature, the current setpoint temperature and the current power.

- Filter changer control. An infrared filter change can occur automatically or be made at the request of the operator. The computer communicates with the filter changer via the serial port using the industry standard MODBUS protocol.
- CCD camera position control. This block controls the position of the camera in three dimensions to provide optimum conditions for obtaining images of the best quality.
- Image acquisition. The block allows one to acquire a video from the CCD camera.
- Image processing and analysis. Image processing and analysis algorithms developed for the THERMO-WET systems can be divided into three groups:
 - image enhancement algorithms;
 - image segmentation algorithms;
 - algorithms for precise measurements of the specimen geometrical properties.

These algorithms ensure high quality processing necessary for accurate measurements of surface properties in the measurement system considered (Strzecha, 2002; Fabijańska, 2007; Koszmider, 2009; Sankowski et al., 2011).

- Physical parameters determination. The block enables one to determine the fundamental physico-chemical parameters of the specimen in the liquid state: the contact angle of the sample material and the surface and the surface tension of the specimen (Strzecha, 2002; Bąkała, 2007; Fabijańska, 2007; Koszmider, 2009; Sankowski et al., 2011).
- Measurements archiving. For the purposes of archiving the results of measurements and source images, the independent SQL database was used.

3.2.1. Project Specification

The main requirements set upon the application may be divided into structural and functional requirements.

The structural requirements specify that the core functional modules of the application should be independent of the physical communication media and the communication protocols used. Moreover, the core functional

modules are expected to form encapsulated entities, with references to the other ones implementing the “uses” relationship of the object-orientation standard. The latter requirement is legitimate in view of the possible re-usage of separate modules in other projects. Specific modules span the image acquisition and processing, and serial port communication.

The functional requirements specify that the application allows for experiment planning and archiving, accounts for dynamic algorithm library linking and conforms to the MODBUS serial communication standard. In addition, the application is expected to provide an interface appropriate for classes of users having access to the desired scope of functionality reflecting different modes in which the experiments may be conducted.

In view of the above-mentioned requirements, the modular structure (Booch et al., 1998) of the application introduces image acquisition and processing library modules, a serial communication module, task scheduling and a user interface module (Sankowski et al., 2006; Strzecha et al., 2006).

3.2.2. Modular Structure

The project distributes the desired functionality between separate modules:

1. The XML processor used as a means of description of storing and loading experiment parameters.
2. The task/experiment-scheduling module responsible for task scheduling and experiment planning.
3. The database module responsible for experiment data storage.
4. The graphical user interface module.
5. The serial communication module responsible for RS-485 communication with the temperature controller and the camera filter adjustment mechanism.
6. The image acquisition module responsible for video camera communication using the frame grabber standard.
7. The image-processing library containing algorithms used for image segmentation and filtering.
8. The image analysis library containing algorithms used for physical and chemical parameter calculation operating on images of the specimen.
9. The mutual dependency between the modules is depicted in Fig. 3.3.

10. The task/experiment scheduler realizes the core control functionality of the application.

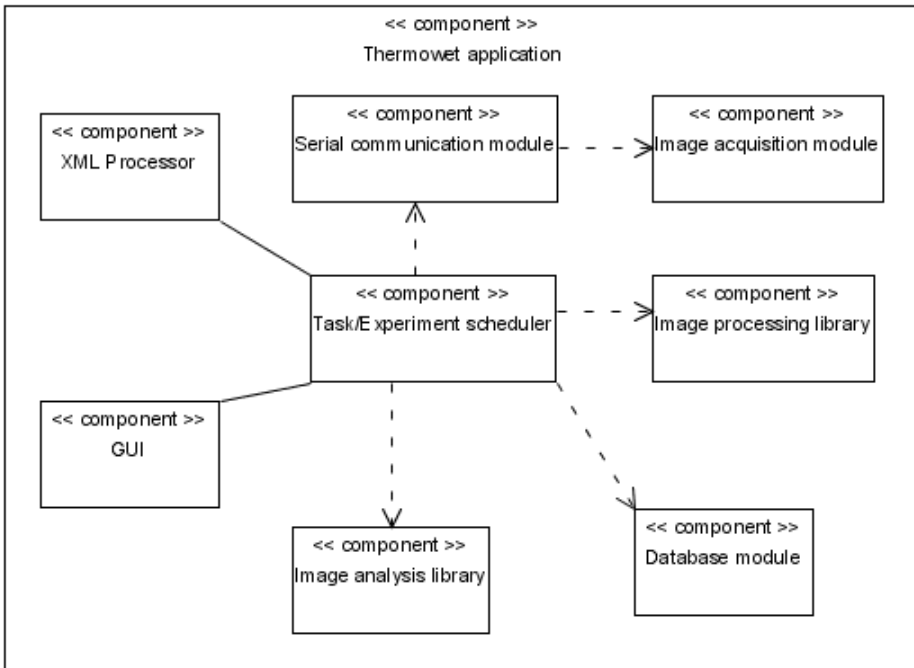


Fig. 3.3. THERMO-WET system's module dependencies

The two out of the seven designed relationships are collaboration relationships rather than implementation dependencies, reflecting the inner design of the main module being dependent on the inner workings of the processing modules with the input/output and the user interface modules being separate entities.

3.2.3. Serial Communication

The serial communication module spans the functionality specific to serial port communication issues as well as higher abstraction level data formatting, including the protocol-specific frame generation. The classes realizing low-level, binary data transmission collaborate with those responsible for device-specific communication. The latter account for being part of an adapter design pattern provides action methods to other modules.

The core entity of the serial communication module is an abstract device driver, reflecting the functionality of a physical device at logical level. The corresponding class is depicted in Fig. 3.4.

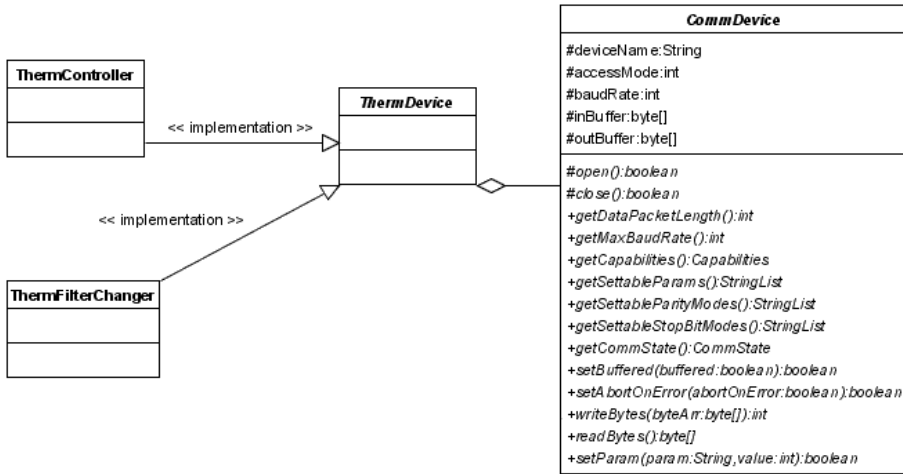


Fig. 3.4. The CommDevice class representing the logical communication device

The abstract driver uses protocol and frame libraries that incorporate the communication standards at a frame communication layer. The abstract device driver is an analogy to the abstract JDBC (Java Database Connectivity) database driver. Therefore, the abstract base driver class defines the universal functionality interface that specific drivers should implement. Moreover, it is expected that there may exist differences between scopes of functionality of drivers controlling different classes of devices, yet using the same low-level communication library.

The abstract device driver is expected to be part of an adapter design pattern, providing collections of action methods to other modules.

The serial communication module distributes the scopes of responsibility involving physical device communication, bit packing and frame formatting among separate classes, incorporating the “uses” object-orientation relationship. Each entity representing a different scope of responsibility is designed as an abstract base class for specific implementations. Each abstract base class is related to the corresponding abstract factory class, resulting in better re-usage possibilities and structural dependencies.

The bridge design pattern is used to separate the logical device entities from the system-specific communication libraries, creating a mutually independent link between the structure and the implementation. The libraries are implemented as subclasses of the main abstract library class, as depicted in Fig. 3.5. This is justified in view of the possible re-usage of the abstract driver classes in projects targeting different host operating systems.

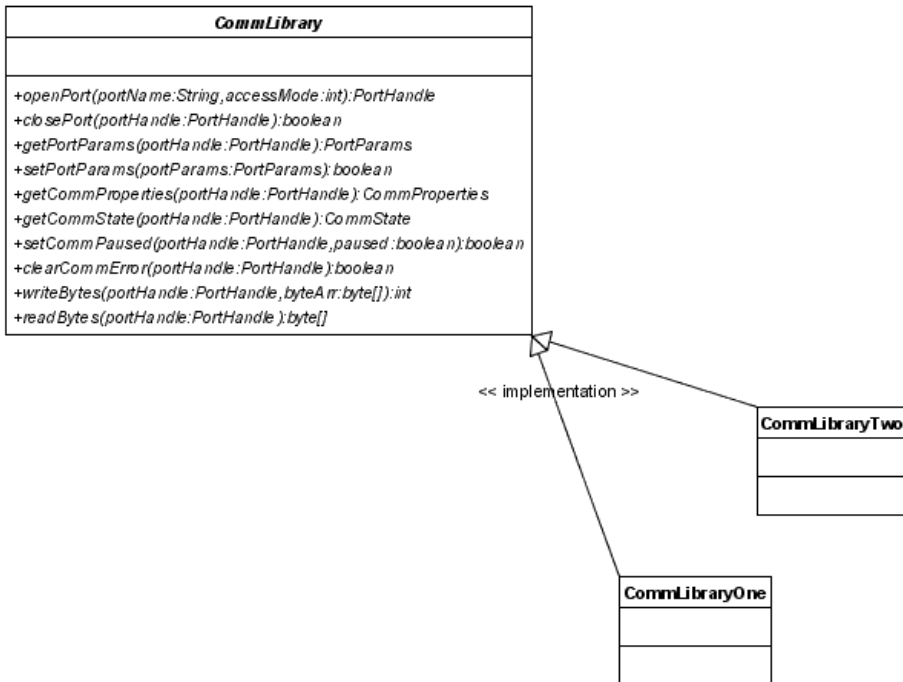


Fig. 3.5. The CommLibrary class realizing the physical implementation of the communication functionality

Many of the communication methods at logical device level are designed to be synchronized using an implicit monitor of the enclosing class. The result structure prevents overlapping calls to communication methods.

The system-specific communication libraries collaborate with the class hierarchies responsible for single-character transmission and frame-level character bundle formatting.

The designed single-character transmission protocol factory is depicted in Fig. 3.6.

The class hierarchy incorporates the two most frequently used transmission modes in control applications, ASCII and RTU, and is sufficiently extensible for the implementation of additional modes, such as UTF-8.

The designed frame-level character bundle formatting factory is depicted in Fig. 3.7. The class hierarchy incorporates the two most frequently used transmission standards in control applications, MODBUS and JBUS and is sufficiently extensible to incorporate other standards.

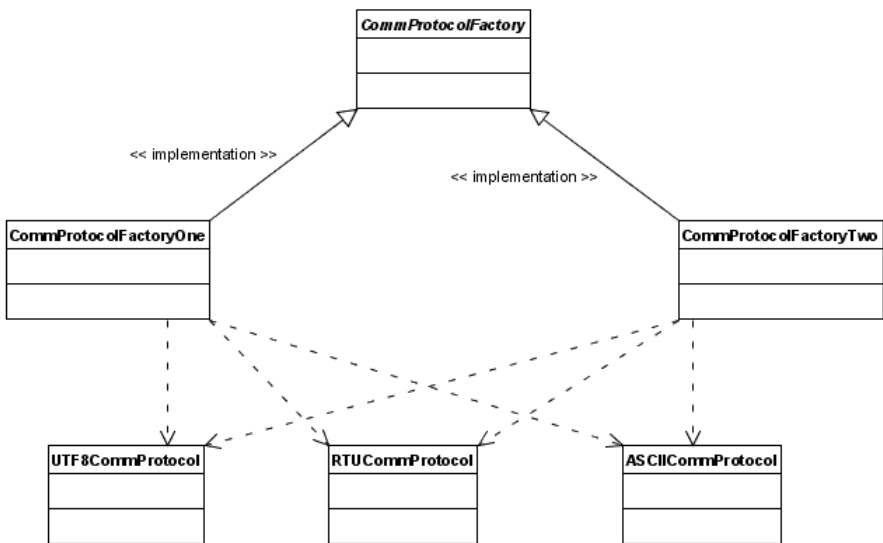


Fig. 3.6. The CommProtocolFactory class incorporating single-character transmission modes

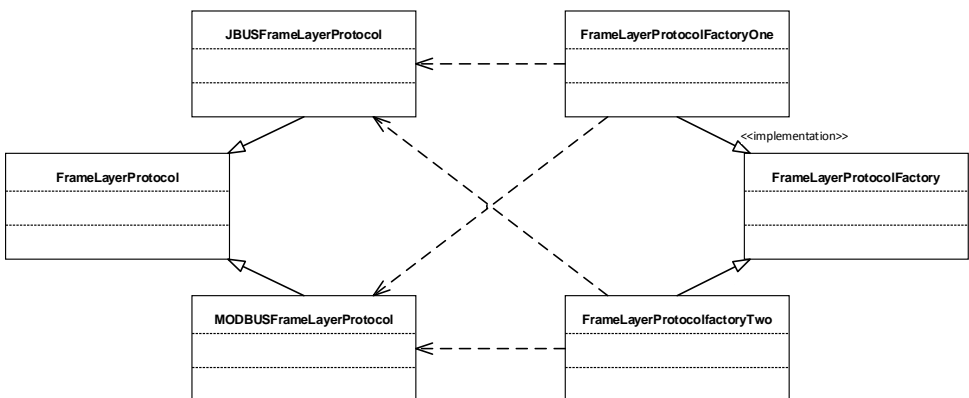


Fig. 3.7. The FrameLayerProtocolFactory class incorporating frame-level character bundle formatting standards

The abstract class representing the logical communication device driver is designed to be inherited from to incorporate the possible physical devices over which the communication may be implemented, as depicted in Fig. 3.8.

The device factories are introduced for further extensibility of the solution to different operating systems.

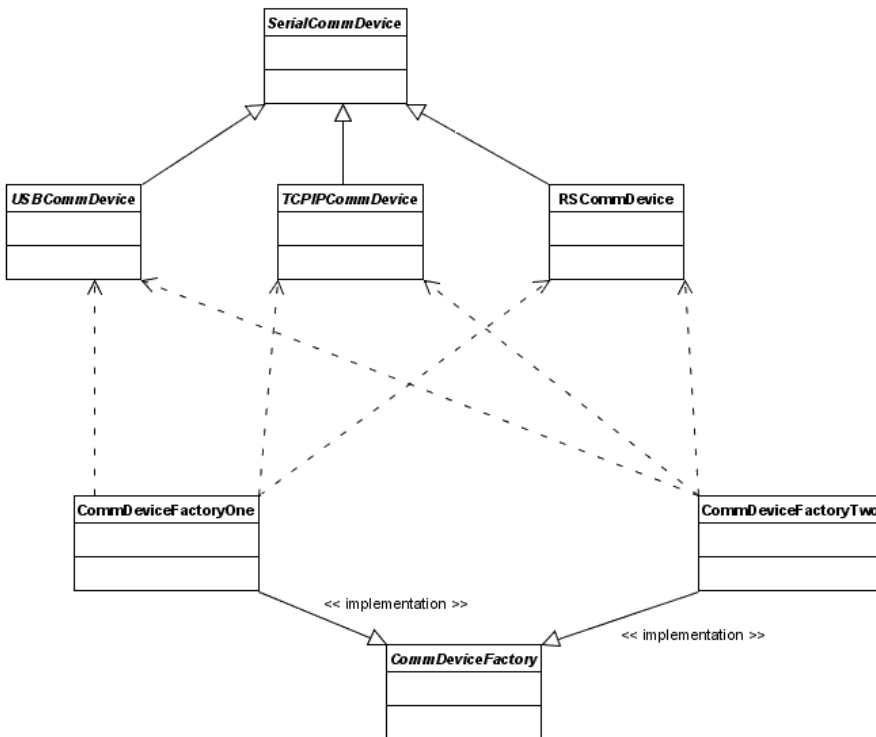


Fig. 3.8. The SerialCommDevice inheriting from the abstract class representing the logical communication device driver

3.2.4. Task Experiment Scheduler Module

The basic requirement set upon the Experiment Scheduler module is to take over the whole control of the THERMO-WET measurement system.

Experiment controlling processes consist of two apart threads, whose responsibility concentrates on a separate device. The functionality of the Task Experiment Scheduler module is depicted in Fig. 3.9.

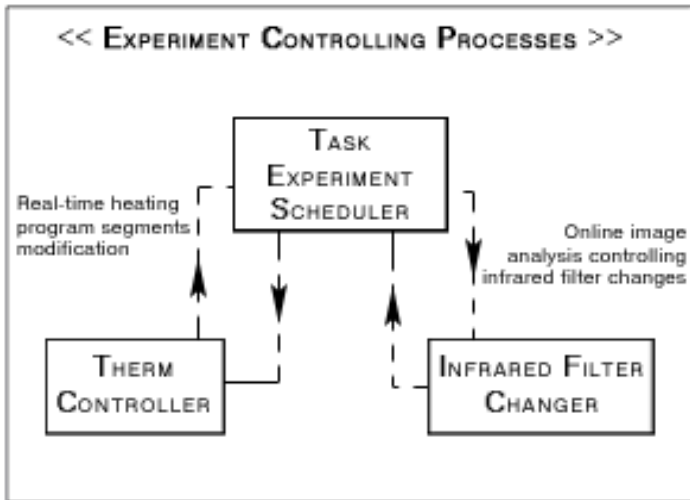


Fig. 3.9. Task Experiment Scheduler functionality

The use of separate therm controller's thread was dictated by the therm controller's tendency to over-control the setpoint temperature. This solution offers the ability to modify a linear temperature rise or change the setpoint temperature of the current program segment.

Online specimen image analysis affords the possibility to change the infrared filter automatically, when the specimen's brightness becomes too high to distinguish it from the feeder's table.

An appropriate choice of an infrared filter is extremely important for precise surface tension and wettability calculations.

The use of the bridge and abstract factory design patterns (Gamma et al., 1995) allows for portable separation between the components realizing the logical and physical functionalities. This is particularly important in the design of industry-dedicated control applications, an example of which is THERMO-WET. The resulting solution is highly maintainable and sufficiently flexible to possible changes that may be introduced during further project development. In particular, the benefits of this approach are indicated in the design of the serial communication module.

4. Image Enhancement

Image analysis is the process of creating a quantitative description of the recorded scene, resulting from the calculations according to the established model of the scene and the optical system. The model should take into account the relationship between the distribution of the intensity of the light in the registered scene containing objects of the considered classes, and the brightness of the digital image. It should also take into account all these side effects factors associated with the imperfection of the camera and electronic components of the vision system that can have a negative impact on the accuracy of the image features measurement. This kind of considerations usually requires the preprocessing of digital images. It must be emphasized that the issue of the image preprocessing is very wide and depends on the specific problem. The result of preprocessing is another digital image, for example, devoid of some of the details of the original one (noise, background) that are not relevant to the analysis, and could hinder it or distort its results. The theory and practice of image processing and analysis use a large number, often conceptually distant, branches of science, such as the theory of linear and non-linear integral transformation, the theory of probability and stochastic processes, estimation theory, statistical decision theory and mathematical morphology (Ballard and Brown, 1982; Gonzalez and Wintz, 1987; Pavlidis, 1987; Jain, 1989; Lim, 1990; Materka, 1991; Chellappa, 1992; Shapiro and Rosenfeld, 1992; Dougherty and Astola, 1993; Teuber, 1993; Baxes, 1994; Dougherty, 1994; Awcock and Thomas, 1995; Watkins et al., 1995; Castleman, 1996; Woźnicki, 1996; Young et al., 1998; Bovik, 2000; Hader, 2000; Shapiro and Stockman, 2000; Zuech, 2000; Nikolaidis and Pitas, 2001; Pitas, 2001; Jahne, 2002; Russ, 2002; Sharma, 2002; Forsyth and Ponce, 2003; Davies, 2004; Jahne, 2004; Jensen, 2004; Acharya and Ajoy, 2005; Umbaugh, 2005; Bauer, 2006; Woods, 2006; Pratt, 2007; Gonzalez and Woods, 2007; Sonka et al., 2007; Sankowski et al., 2011).

It should be underlined that there is a strong relationship between the quality of image segmentation and the accuracy of surface property determination. An algorithm computing a wetting angle and surface tension performs its task on the basis of specimen shape analysis, so the stage of image segmentation is to determine the specimen edges and the upper

edge of the base plate localization as accurately as possible. However, in the case of the selected segmentation algorithm, accurate image segmentation is only guaranteed by proper image enhancement algorithm selection.

Preprocessing algorithms developed for the THERMO-WET vision system aim at correcting factors arising from the CCD chip imperfections and the specificity of high-temperature measurements. In particular, they include:

- the removal of the instrumental background;
- the compensation of the pixel non-uniform response;
- the removal of the aura;
- the noise filtering

These steps are described in details in the following subsections.

4.1. Removal of Instrumental Background

An instrumental background is an additional signal appearing in every digital image which consists of a bias signal and a thermally generated charge (dark current). It can seriously affect the quality of digital images. In images obtained from the THERMO-WET system the instrumental background manifests itself by vertical lines of non-uniform intensity (Fig. 4.1a). In order to diminish the influence of the instrumental background, an algorithm constructing its approximate image from a set of dark frames (images obtained with the closed shutter) was developed. A master dark frame – the approximate image of the instrumental background is presented in Fig. 4.1b. The correction is simply the subtraction of the master dark frame from the original image. The result of instrumental background removal is presented in Fig. 4.1c.

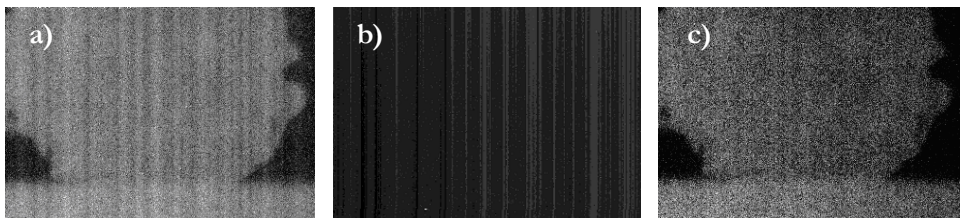


Fig. 4.1. Instrumental background elimination; a) original image, copper, 817°C; b) master dark – after histogram stretching; c) corrected image

It should be emphasized that master dark frame construction used in the THERMO-WET system is not simply input dark frames averaging. The developed algorithm operates iteratively. A set of input dark frames is averaged in successive iterations in order to extract dominant components of the instrumental background. The average frame is then subtracted from each of the input frames in order to build an input set for the next iteration. The process is repeated until there are no distortions in the average frame. A block diagram of the algorithm is presented in Fig. 4.2.

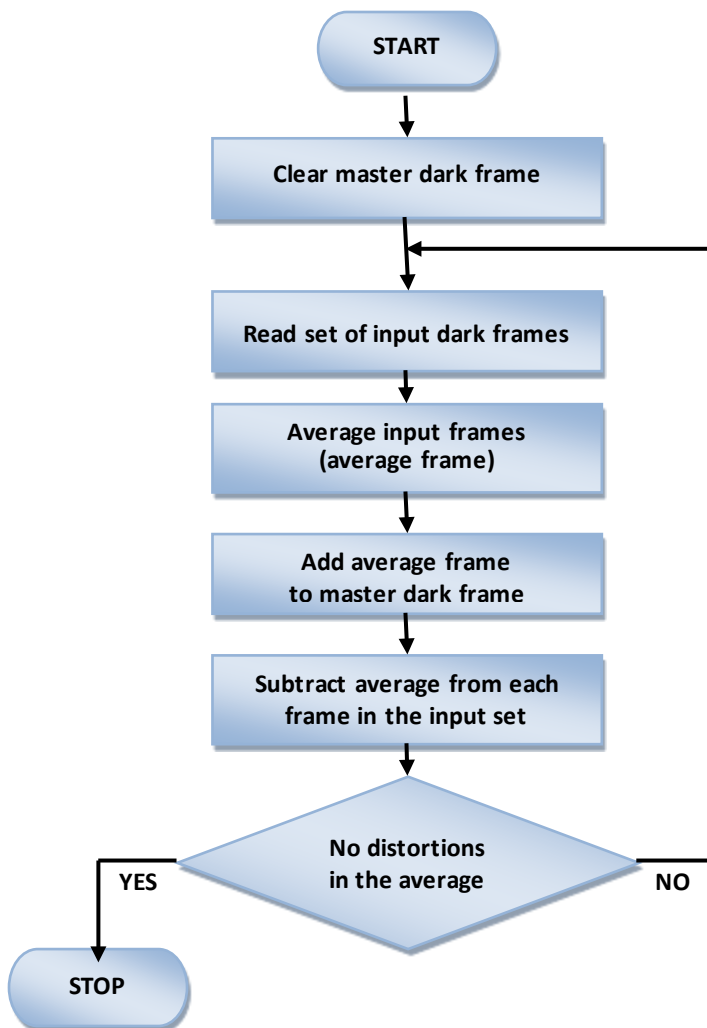


Fig. 4.2. Flow diagram of master dark frame construction algorithm

4.2. Compensation of Pixel Non-uniform Response

For the correction of the non-uniform pixel response, an adaptation of the astronomical method (Howell, 2006) was proposed. The method called flat-fielding is the division of an original image by a flat-field (which is an image of a uniformly illuminated surface) in accordance with the following equation:

$$L' = \bar{L}_{ff} \frac{L - L_b}{L_{ff} - L_b}; \quad (4.1)$$

where:

L' – the corrected image;

L – the original image;

L_b – the image of the instrumental background;

L_{ff} – the flat field (map of pixel sensitivities);

\bar{L}_{ff} – the average intensity of the flat field.

In order to eliminate random distortions an average of several frames was used as a master flat field. The results of the flat field correction applied to an exemplary image obtained from the THERMO-WET vision system are presented in Fig. 4.3.

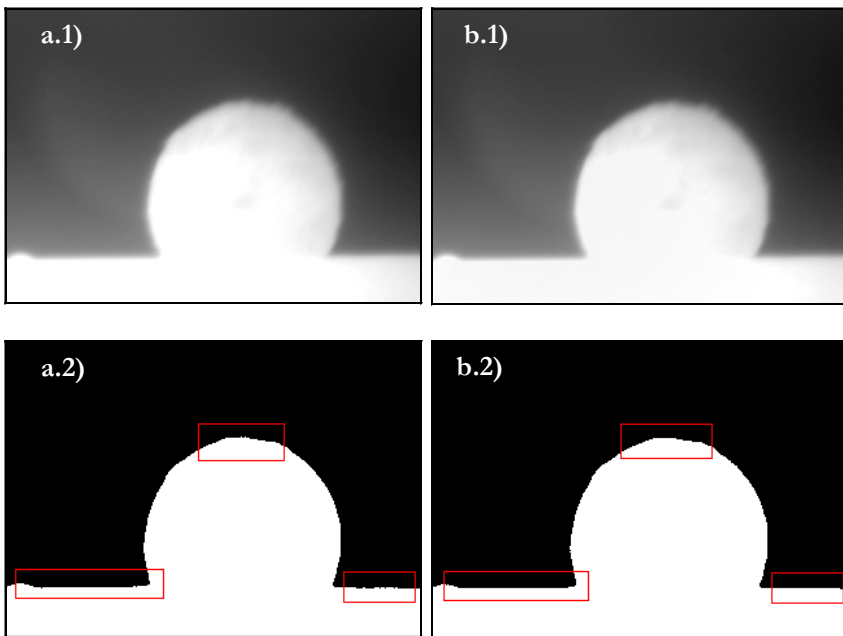


Fig. 4.3. Compensation of pixel non uniform sensitivity; a) original image, copper, 10940°C; image after correction; 1) image before segmentation; 2) image after segmentation

The comparison is made by means of image segmentation quality. Important details in the specimen shape projection are highlighted by rectangular frames.

The results presented in Fig. 4.3 show that flat-fielding improves the quality of the specimen shape projection due to image segmentation. In the case of original images, the improvement of image quality seems to be rather poor. The actual image quality improvement can be seen in images after segmentation. Preceding the segmentation by flat-fielding significantly increases the accuracy of the specimen shape projection. Objects after segmentation are characterized by smoother and more continuous edges than in the case of no flat-fielded corrected images. It should be stressed that the differences in the accuracy of specimen edges projection are important from the point of view of the specimen shape analysis carried out in the following stage of the measurement process.

4.3. Automatic Change of Optical Filters

The specificity of high-temperature measurements requires the use of optical filters. In particular, infrared (IR) and neutral density (ND) filters are applied. They block mid-infrared wavelengths (thermal radiation) and reduce the intensity of light. It should be underlined that only the selection of proper filter allows measurements. The problem is illustrated in Fig. 4.4.

The THERMO-WET vision system enables one to obtain images in the following filter configurations: FILTER 0 – no filter; FILTER 1 – NG4 3.0 mm (IR filter); FILTER 2 – NG4 4.0 mm+BG38 1.0 mm (IR and ND filter).

During the measurements filters must be changed together with properties of the images obtained. The moment of filter change was determined by the measurement system operator. However, an algorithm of filter automatic change was developed. The algorithm analyzes changes of the image contrast. In Fig. 4.5 a change in the image contrast as a function of time (and in consequence, of temperature) is shown. Images obtained without a filter (FILTER 0) were also considered. Images corresponding to the characteristic points marked on the curve are presented in Table 4.1.

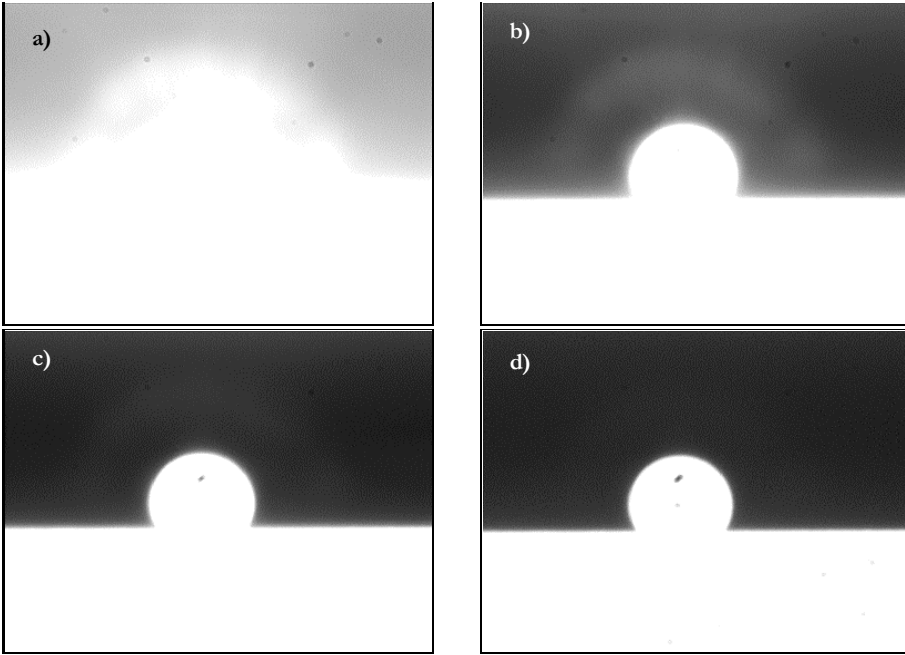


Fig. 4.4. Influence of optical filter selection on image quality; a) original image, palladium, 1564°C; b) and c) improper filter selection; d) proper filter selection

During the measurements filters must be changed together with properties of the images obtained. The moment of filter change was determined by the measurement system operator. However, an algorithm of filter automatic change was developed. The algorithm analyzes changes of the image contrast. In Fig. 4.5 a change in the image contrast as a function of time (and in consequence, of temperature) is shown. Images obtained without a filter (FILTER 0) were also considered. Images corresponding to the characteristic points marked on the curve are presented in Table 4.1.

It can easily be seen (Fig. 4.5, Tab. 4.1) that together with a temperature growth, the contrast of the images obtained with FILTER 0 increases to reach the maximum and then rapidly falls to a zero value, which corresponds to the saturation of CCD photosensitive elements. The best quality images are obtained for the maximum contrast value. The curves of contrast as a function of time/temperature obtained for FILTER 1 and FILTER 2 have a similar character (see Fig. 4.6).

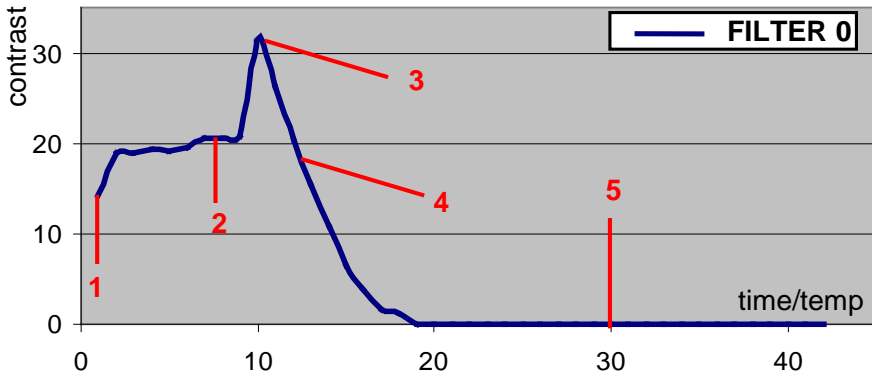


Fig. 4.5. Change of image contrast in function of temperature. Images obtained without filter (FILTER 0) are considered

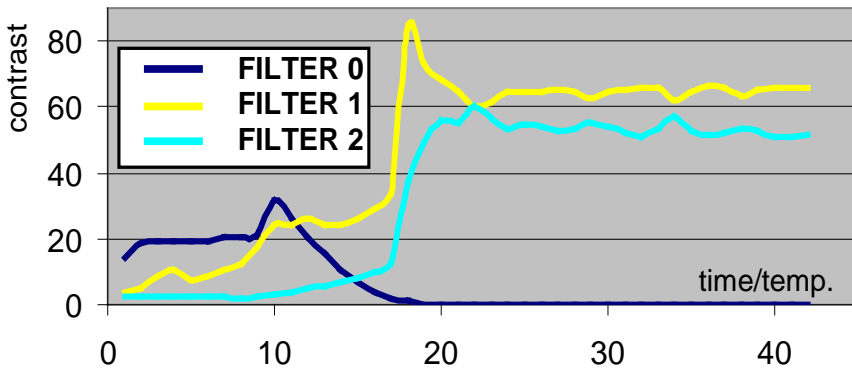

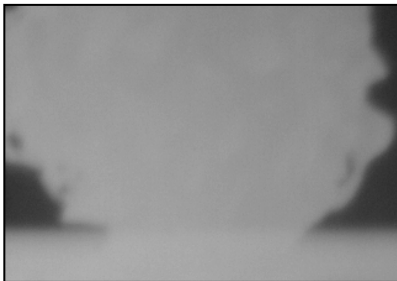


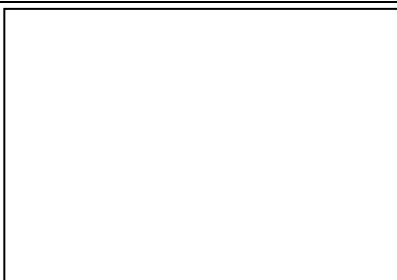


Fig. 4.6. Change of image contrast as a function of temperature for all filters from THERMO-WET vision unit

Table 4.1. Images corresponding with points marked on curve from Fig.4.5

1		<p>copper, 553⁰C no filter</p>
2		<p>copper, 695⁰C no filter</p>
3		<p>copper, 743⁰C no filter maximum contrast</p>
4		<p>copper, 769⁰C no filter</p>
5		<p>copper, 1300⁰C no filter saturation of CCD photosensitive elements</p>

Moreover, when the contrast of an image obtained with weaker filter decreases after crossing the maximum, the contrast of images acquired with a stronger filter starts to increase. Therefore, a change of the current filter into the stronger one should be made after the maximum contrast is crossed. On this assumption, the proposed algorithm of automatic filter change is based. Experiments proved that in the case of the analyzed images, a 10% decrease in the contrast value means that its maximum was crossed. Block diagram of the algorithm of automatic filter change is presented in Fig. 4.7 and block diagram of the algorithm of maximum contrast value detection is presented in Fig. 4.8.

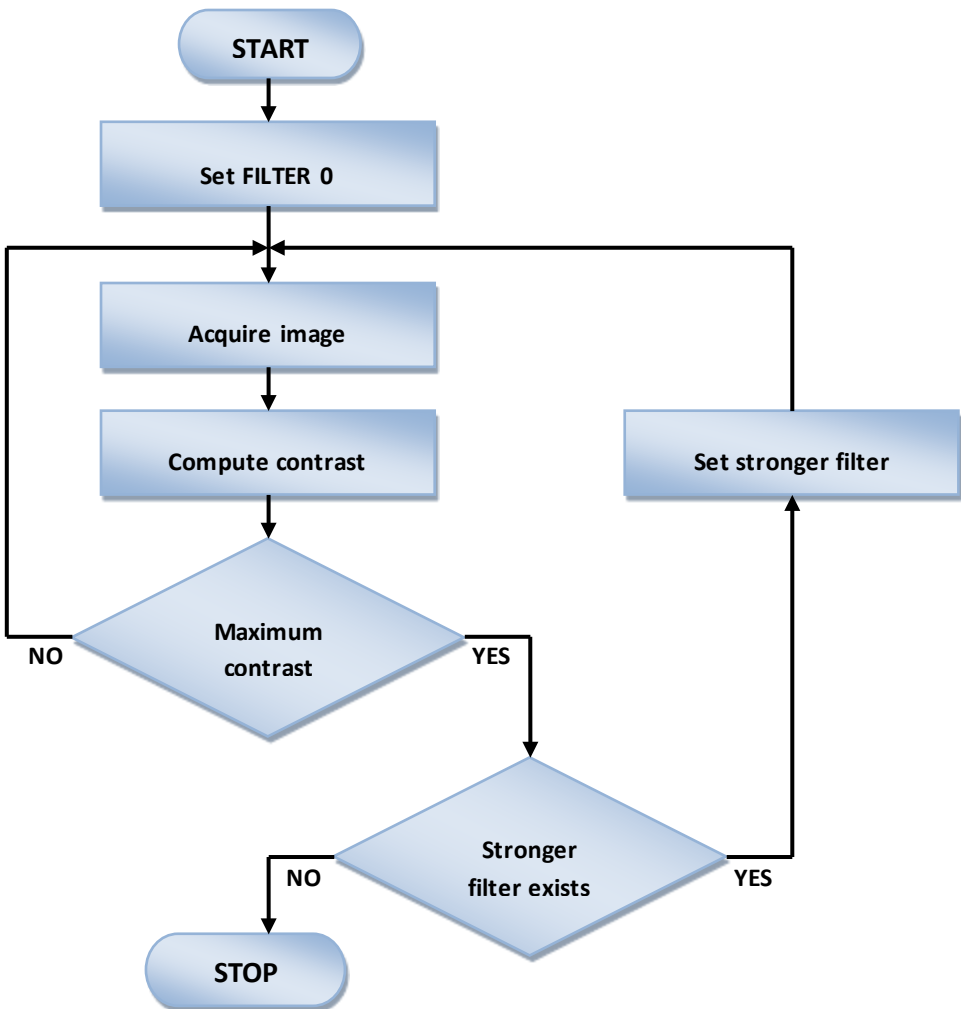


Fig. 4.7. Block diagram of algorithm of optical filters automatic change

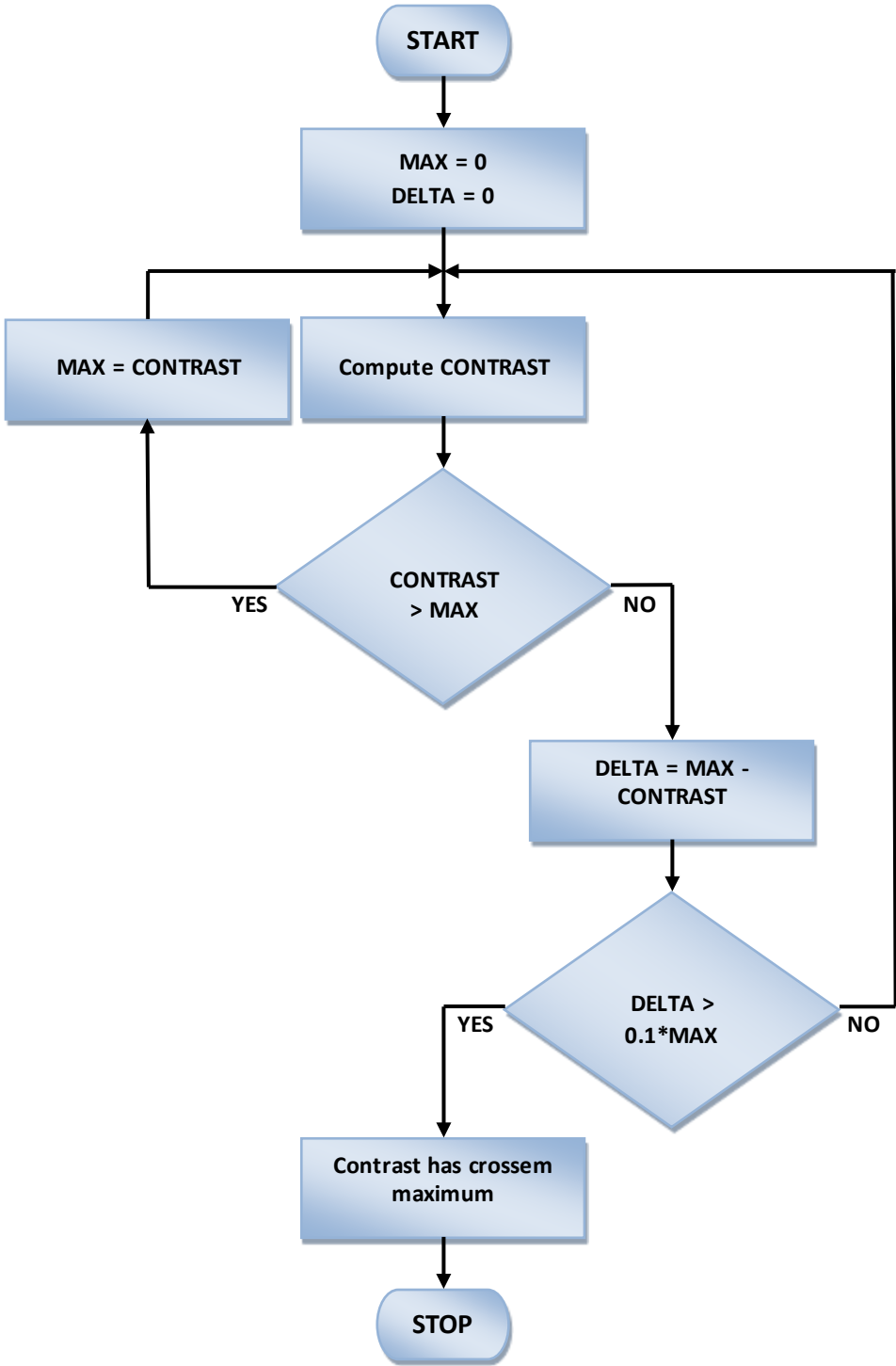


Fig. 4.8. Block diagram of algorithm of contrast maximum crossing detection

4.4. Switching Median Filter

Digital images can often be corrupted by noise. It manifests itself by erroneous signal fluctuations. Noise presence can seriously affect the quality of digital images – in particular, the degradation of image spatial resolution can be observed. Therefore, it is essential to detect and correct noisy pixels before the main processing. Numerous approaches have already been developed for noise removal. In general, they can be divided into two main groups: image filtration and image averaging.

During filtration, an image is either convolved with an appropriately selected mask or non-linearly filtered (Pitas and Venetsanopou, 1990). However, filtration sacrifices temporal resolution as it affects the blurred appearance of the image and, as a result, compromises the level of details. Averaging is said to reduce the noise level without compromising details. However, it involves at least several images of the observed scene and, in consequence, cannot be used when the view of the field changes rapidly.

Despite the variety of existing techniques, one of the most popular methods for noise removal is median filtration (Dougherty and Astola, 1993). In this method the pixel situated in the center of the odd-sized mask is substituted with the median value of other pixels under the mask. Despite its popularity, there are some drawbacks to the median filtration. First of all, it compromises details of the image and in consequence makes it look blurry. Therefore, many modifications of the classical median filtration were developed, described for example in (Huang, 1981; Pitas and Venetsanopou, 1990; Gil and Werman, 1993; Guangjin and Jiegu, 1997; Wu and Horng, 2003; Kravchonok et al., 2007; Lee et al., 2007). In general, they involve different techniques, which allow one to determine noise-corrupted pixels and decrease the number of pixels subjected to median filtration. Vector median filters (Smolka et al., 2001; Morillas et al., 2005; Smolka, 2007), weighted median filters (Yin et al., 1996; Wirth and Nikitenko, 2005), matrix-valued median filters (Welk et al., 2003; Welk et al., 2005) or relaxed median filters (Hamza et al., 1999) may be mentioned as examples of traditional approach modifications.

Recently, fuzzy techniques and neural networks (Lee et al., 2004; Alajlan and Jernigan, 2004; Schulte et al., 2005; Toprak and Guler 2006) have also become popular in determining which pixels should be subjected to median filtration.

One of the possible solutions to the problems mentioned above is the so-called "decision-based" or "switching" filters (Sun and Neuvo, 1994; Abreu et al., 1996; Eng and Ma, 2001; Chan et al., 2004; Chan et al., 2005; Garnett et al., 2005; Ng and Ma, 2006; Fabijańska and Sankowski, 2007). The concept is to divide the image restoration process into two stages. In the first stage the map of disturbed pixels is constructed. The second stage is a process of image filtration (using a linear or a median filter) similar to the conventional one. However, only pixels considered as corrupted by noise are subjected to filtration.

In this chapter a new approach to the construction of the noisy pixels map is presented. In order to identify noisy pixels, a simple statistical analysis of pixel context is carried out. The analysis allows one to classify pixels as corrupted and uncorrupted ones, so as to avoid the damage of pixels not affected by noise. In consequence, the noisy pixels can be effectively corrected while preserving the detailed image information at the same time. Particular attention is paid to the high quality of image restoration.

Algorithm Description

In digital images, noise manifests itself as local gray-levels fluctuations. Noisy pixels are single pixels significantly brighter or significantly darker than their neighborhood. Assuming Gaussian distribution of pixel brightness fluctuations, they can be detected as ones of values significant different from the mean brightness in their context.

The proposed algorithm works in two stages:

- construction of a map of disturbed pixels;
- correction of the pixels indicated by the map.

In the first stage of the algorithm for all pixels of the image mean value (4.2) and standard deviation (4.5) of brightness in their local areas are calculated.

$$\mu(x, y) = \frac{\sum_{i=-a}^a \sum_{j=-b}^b L(x+i, y+j)}{m * n}; \quad (4.2)$$

$$a = \left\lfloor \frac{m}{2} \right\rfloor; \quad (4.3)$$

$$b = \left\lfloor \frac{n}{2} \right\rfloor; \quad (4.4)$$

where:

$L(x, y)$ – the pixel brightness;

x, y – the spatial coordinates of the pixel;

m, n – dimensions of the local area.

$$\sigma(x, y) = \sqrt{\frac{\sum_{i=-a}^a \sum_{j=-b}^b (L(x+i, y+j) - \mu(x, y))^2}{m * n}}. \quad (4.5)$$

On the basis on the calculated values, a map of disturbed pixels is constructed according to the following rule:

$$d(x, y) = \begin{cases} 1 & \text{for } |L(x, y) - \mu(x, y)| > \sigma(x, y) \\ 0 & \text{for } |L(x, y) - \mu(x, y)| \leq \sigma(x, y) \end{cases}. \quad (4.6)$$

Additionally, to improve the filter ability to preserve image details, every pixel is checked to determine whether it belongs to a larger structure in the scene. If it does, it needs to be removed from the constructed map. This test is also provided on the basis of statistical distribution of brightness in the pixel neighborhood. The pixel is removed from the disturbed pixels map if any of the following conditions is fulfilled by its brightness value:

$$|L(x, y) - L(x-1, y)| < d(x, y) \wedge |L(x, y) - L(x+1, y)| < d(x, y); \quad (4.7)$$

$$|L(x, y) - L(x, y-1)| < d(x, y) \wedge |L(x, y) - L(x, y+1)| < d(x, y); \quad (4.8)$$

$$|L(x, y) - L(x-1, y-1)| < d(x, y) \wedge |L(x, y) - L(x+1, y+1)| < d(x, y); \quad (4.9)$$

$$|L(x, y) - L(x-1, y+1)| < d(x, y) \wedge |L(x, y) - L(x+1, y-1)| < d(x, y). \quad (4.10)$$

In the next step of the algorithm, pixels indicated in the noise map are corrected. The correction is made by substituting the gray-level of the indicated pixels by the median value of their closest neighbors.

In most cases, not all of the disturbed pixels are recognized and corrected in one pass of the algorithm. Generally, the process should undergo several iterations until better image restoration is obtained.

Experimental Results

Exemplary results of the noise removal using the proposed algorithm are presented for three test images. Two of them (Image 1 and Image 2) were obtained from the THERMO-WET system during the normal measurement process. The third test image (Image 3) contains simple geometric structures and was specially prepared to test different noise removal algorithms, especially their ability to preserve image details. Uncorrupted test images are presented in Fig. 4.9.

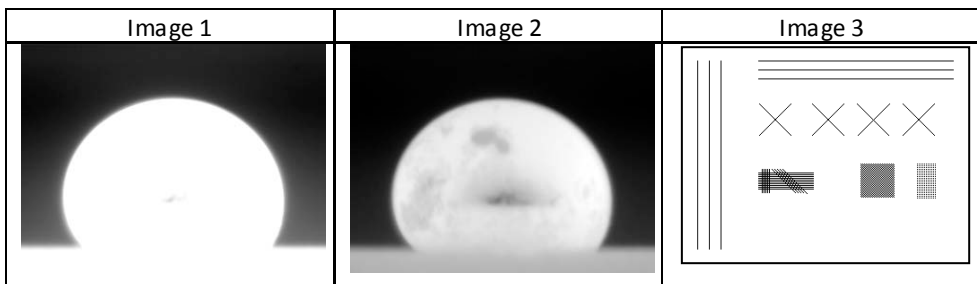


Fig. 4.9. Uncorrupted test images used in the tests of proposed filtration algorithm

Two types of noise were added to the test images: Gaussian and salt-and-pepper ones. The Gaussian noise (thermal noise) is usually the main part of noise originating from the digital camera sensor. It is additive, independent of each pixel and independent of the signal intensity (Nakamura, 2005). Salt-and-pepper noise (impulsive noise, spike noise) is fat-tail disturbed and can be caused by analog-to-digital converter errors, bit errors in transmission, and so forth. (Boncelet, 2005).

The Gaussian noise added to the test images were characterized by a zero mean value and deviation equal to 5, 10 and 15. Corrupted images are presented in Fig. 4.10. Additionally in Fig. 4.11 the test images corrupted with salt-and-pepper noise of levels 10% and 30% are shown.

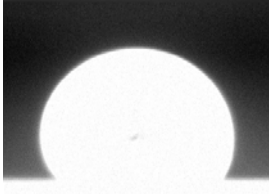
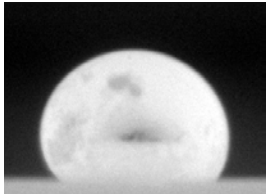
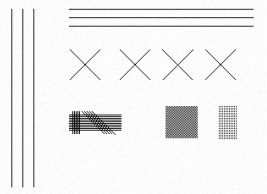
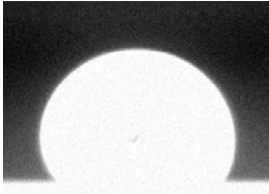
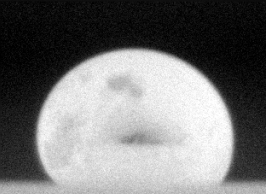
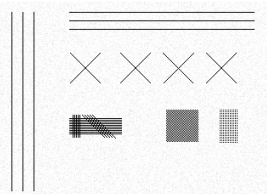
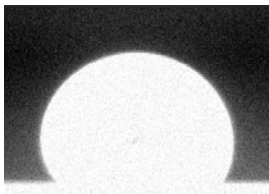
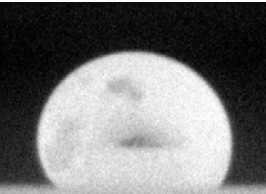
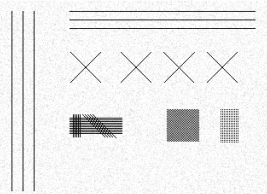
	Image 1	Image 2	Image 3
Deviation: 5			
Deviation: 10			
Deviation: 15			

Fig. 4.10. Test images corrupted by Gaussian noise

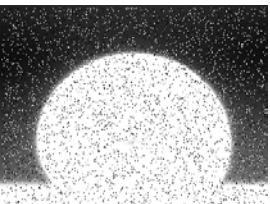
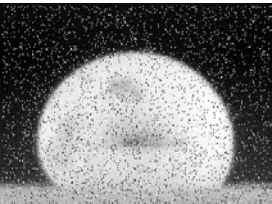
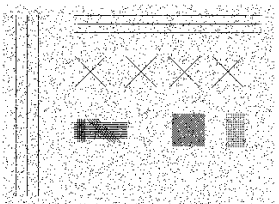
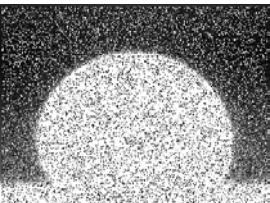
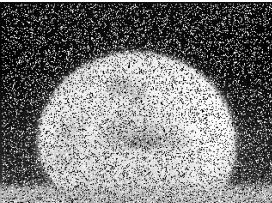
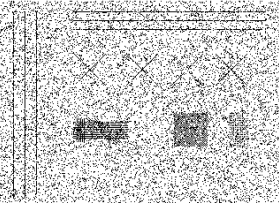
	Image 1	Image 2	Image 3
Noise level: 10%			
Noise level: 30%			

Fig. 4.11. Test images corrupted by salt-and-pepper noise

The noised test images were processed with the following methods:

1. the proposed method based on the statistical disturbed pixels map;
2. the noise removal method based on the minimum/maximum disturbed pixels map described in (Fabijańska and Sankowski, 2011);
3. the median filter with a 3×3 mask size;
4. the median filter with a 5×5 mask size.

All the calculations for the proposed algorithm were made using the local area size $m = n = 3$. Higher sizes increase algorithm computational complexity without significant improvement of noise removal quality.

In order to quantify the noise level the signal-to-noise ratio (SNR) and the mean square error (MSE) are used (Pitas and Venetsanopou, 1990). The lower the MSE and the higher the SNR value the better quality of the analyzed image.

The mean square error can be defined as follows:

$$MSE = \frac{\sum_{x=0}^{N-1} \sum_{y=0}^{M-1} (L(x, y) - L'(x, y))^2}{N * M}. \quad (4.11)$$

where:

$L'(x, y)$ – the brightness value of a pixel in a corrupted image;

N, M – the horizontal and vertical image resolution.

The signal-to-noise ratio is given by the equation:

$$SNR = 20 \log_{10} \sqrt{\frac{\frac{1}{N * M} \sum_{x=0}^{N-1} \sum_{y=0}^{M-1} L(x, y)^2}{MSE}}. \quad (4.12)$$

The image restoration results obtained are juxtaposed in Tables 4.2 and 4.3. In Table 4.2 the Gaussian noise removal results are presented and in Table 4.3 the results of salt-and-pepper noise removal are shown. The first column in every table indicates the method used for noise removal and the following ones the results obtained for different noise parameters. All the methods were iteratively repeated (but not more than 20 times) to obtain the best image restoration. The number of iterations i for which the best result was achieved is presented together with the calculated MSE and SNR measures. For the noise removal method based on the minimum/maximum disturbed pixels map a discrimination level $l = 9$ was used (Fabijańska and Sankowski, 2012).

Table 4.2. Gaussian noise removal results

Image 1						
	Deviation: 5		Deviation: 10		Deviation: 15	
	MSE	SNR	MSE	SNR	MSE	SNR
None	19.35	32.48	74.45	26.58	163.00	23.12
Median 3×3	2.42	41.55	5.84	37.72	10.63	35.11
	<i>i</i> = 19		<i>i</i> = 17		<i>i</i> = 20	
Median 5×5	2.21	41.95	4.36	38.99	6.93	36.98
	<i>i</i> = 2		<i>i</i> = 4		<i>i</i> = 6	
Min/Max maps	5.38	38.06	15.64	33.39	30.48	20.45
	<i>i</i> = 20		<i>i</i> = 20		<i>i</i> = 20	
Statistical map	3.85	39.55	11.18	34.91	21.69	32.02
	<i>i</i> = 13		<i>i</i> = 18		<i>i</i> = 17	
Image 2						
	Deviation: 5		Deviation: 10		Deviation: 15	
	MSE	SNR	MSE	SNR	MSE	SNR
None	23.71	30.03	87.00	24.39	182.99	21.16
Median 3×3	3.25	38.65	7.24	35.17	12.86	32.68
	<i>i</i> = 14		<i>i</i> = 18		<i>i</i> = 20	
Median 5×5	2.86	39.21	5.27	36.55	8.07	34.70
	<i>i</i> = 2		<i>i</i> = 4		<i>i</i> = 5	
Min/Max maps	6.84	35.41	17.31	31.36	32.00	28.68
	<i>i</i> = 12		<i>i</i> = 20		<i>i</i> = 20	
Statistical map	5.77	36.16	16.25	31.66	31.54	28.78
	<i>i</i> = 14		<i>i</i> = 19		<i>i</i> = 19	
Image 3						
	Deviation: 5		Deviation: 10		Deviation: 15	
	MSE	SNR	MSE	SNR	MSE	SNR
None	13.93	36.42	51.72	30.67	113.44	27.19
Median 3×3	1884.05	15.26	1845.87	15.32	1814.00	15.37
	<i>i</i> = 2		<i>i</i> = 2		<i>i</i> = 2	
Median 5×5	1890.45	15.25	1862.44	15.29	1839.83	15.32
	<i>i</i> = 1		<i>i</i> = 1		<i>i</i> = 1	
Min/Max maps	1332.15	16.68	1261.16	16.85	1263.31	16.77
	<i>i</i> = 1		<i>i</i> = 1		<i>i</i> = 1	
Statistical map	451.86	21.36	459.86	21.24	476.42	21.05
	<i>i</i> = 1		<i>i</i> = 1		<i>i</i> = 1	

Table 4.3. Salt-and-pepper noise removal results

Image 1				
Method	Noise level: 10%		Noise level: 30%	
	MSE	SNR	MSE	SNR
None	2700.00	11.07	8041.66	6.26
Median 3×3	1.78	42.93	6.89	37.04
	<i>i</i> = 2		<i>i</i> = 5	
Median 5×5	2.09	42.21	5.77	37.81
	<i>i</i> = 2		<i>i</i> = 3	
Min/Max maps	0.70	47.00	4.74	38.67
	<i>i</i> = 1		<i>i</i> = 4	
Statistical map	0.83	46.19	4.53	38.87
	<i>i</i> = 3		<i>i</i> = 4	
Image 2				
Method	Noise level: 10%		Noise level: 30%	
	MSE	SNR	MSE	SNR
None	2534.98	9.92	7528.74	5.43
Median 3×3	2.24	40.30	6.78	35.48
	<i>i</i> = 2		<i>i</i> = 4	
Median 5×5	2.48	39.85	6.50	35.67
	<i>i</i> = 2		<i>i</i> = 2	
Min/Max maps	0.75	45.07	4.50	37.26
	<i>i</i> = 1		<i>i</i> = 3	
Statistical map	1.06	43.55	4.26	37.51
	<i>i</i> = 3		<i>i</i> = 6	
Image 3				
Method	Noise level: 10%		Noise level: 30%	
	MSE	SNR	MSE	SNR
None	3133.56	12.78	9437.94	7.54
Median 3×3	2306.36	14.42	2531.57	14.00
	<i>i</i> = 2		<i>i</i> = 2	
Median 5×5	2235.23	14.56	2378.32	14.30
	<i>i</i> = 1		<i>i</i> = 1	
Min/Max maps	2306.36	14.42	2531.57	14.00
	<i>i</i> = 2		<i>i</i> = 2	
Statistical map	887.32	18.48	1978.69	15.02
	<i>i</i> = 1		<i>i</i> = 2	

	Image 1	Image 2	Image 3
Original image			
Corrupted image			
Median 3x3			
Median 5x5			
Min/max map			
Min/max map			

Fig. 4.12. Comparison of restoration results for test images corrupted by Gaussian noise of deviation equal to 15

	Image 1	Image 2	Image 3
Original image			
Corrupted image			
Median 3x3			
Median 5x5			
Min/max map			
Min/max map			

Fig. 4.13. Comparison of restoration results for test images corrupted by salt-and-pepper noise of level 30%

Exemplary resulting images of the test images restoration using the filters mentioned above are presented in Figs 4.12 and 4.13. For better presentation the images of the highest corruption level were selected. Based on the results shown it can be concluded that for images corrupted with salt-and-pepper-noise introduced approach to image enhancement affects with significant signal-to-noise ratio and mean square error improvement. The results obtained are usually far better than in the case of all the traditional approaches tested and those similar to the ones of the method based on minimum/maximum maps; for every noise level a significant increase in the reconstructed image quality can be observed.

In the case of images corrupted with Gaussian noise, the method proposed, like other “switching filters”, has a much weaker ability to remove noise than traditional median filters. This is related to a much higher difficulty in identifying pixels affected by noise.

Moreover, it should be underlined that in the case of the proposed filtration method most of image information is preserved even for a very high noise level. The sharpness of the result images and the detail level are far better than those obtained with the use of other methods. All the other tested methods of noise removal compromise details. Their application makes a reconstructed image look blurry and unsharp and additionally, a significant part of the information contained in the image can be lost.

The results presented indicate that the proposed approach can be useful in the case of images corrupted by fixed-valued (salt-and-pepper) noise. In such a case, it usually provides much better results than many other well-known methods.

5. Correction of the Image Distortions Influenced by the Gas Flow

For most materials, measurements of the surface tension and the wetting angle are carried out in a protective atmosphere. The flow of protective gas introduces significant distortions to the acquired images (Strzecha et al., 2012). Gas, of a temperature of approximately 0°C, is introduced to the furnace chamber from the side of the CCD camera and then, on its way to the specimen it is heated to the current working temperature of, for example, 1500°C.

The absolute index of the light refraction n in gas depends on its density and temperature. For the temperature above 0°C and for the atmospheric pressure, it is given by the equation:

$$\Delta n = \frac{k_1 \gamma}{T}; \quad (5.1)$$

where:

γ – the density of gas;

T – the absolute temperature;

k_1 – the constant value.

Boyle-Mariotte's law states that for a constant pressure the gas density is inversely proportional to its absolute temperature:

$$\Delta n = \frac{k_2}{T^2}; \quad (5.2)$$

where:

k_2 – the constant value.

Following formula (5.2), in the example above, where the temperature of gas rises from 0°C to 1500°C on its way through the furnace chamber, the value of Δn decreases nearly 40 times.

Hence, we can assume that the gas introduced to the furnace should be considered the optical lens, whose index of light refraction smoothly changes between the camera and the specimen.

It should be pointed out that the presented model of “gas lens” is very simplified. In fact, parameters of this lens depend on many different factors, including: parameters of the gas flow, the composition of the gas mixture and the distribution of temperature in the furnace chamber.

Additionally, these parameters usually change during measurement experiments. As a result, the lens formed by the protective gas atmosphere becomes an important part of the vision system, introducing significant distortions to the images.

The phenomenon described above is not only related to the flow of protective gas in the heating chamber of the furnace, which has an impact on the quality of the acquired images and, consequently, the accuracy of the measurements.

Fig. 5.1 shows the presumed distribution of isotherms in the gas laminar flowing through the heating chamber of the furnace.

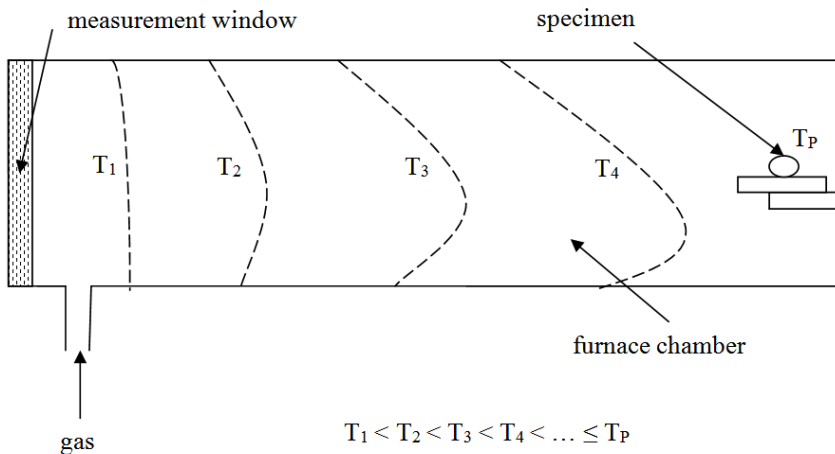


Fig. 5.1. Presumed distribution of isotherms in the gas laminar flowing through the heating chamber of the furnace (Strzecha et al., 2012)

In the area adjacent to the measurement window the gas has a temperature close to room temperature (isotherm T1). Flowing into the furnace chamber, the gas is heated by the furnace walls, but subsequent isotherms are not characterized by axial symmetry because the colder parts of the gas will flow closer to the bottom of the chamber. However, in a horizontal plane such symmetry will occur. Thus, the optical properties of the gas on the way from the measurement window to the specimen will not have axial symmetry. As a result, the vertical and the horizontal transfer of an image differ from each other, which affects the shape of the recorded drop. The higher the temperature at which the measurement is carried out, the greater the deformation of the specimen observed.

Another phenomenon caused by the flow of protective gas, and significantly impedes the measurement of the geometric dimensions of the specimen is the phenomenon of aura shown in Fig. 5.2 (Strzecha et al., 2012).

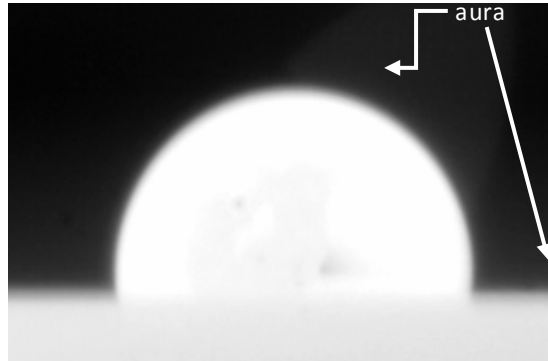


Fig. 5.2. The phenomenon of aura around a specimen and the surface of the measurement table

In the image, it is clear that the phenomenon of aura has a significantly lower thickness and clarity on the contour of the drop than the tray table. This observation led to formulate the hypothesis that this phenomenon is the result of a "fata morgana".

On the border between two media with different speed of light, the following relation is fulfilled:

$$\frac{\sin(\alpha_1)}{\sin(\alpha_2)} = \frac{V_1}{V_2}; \quad (5.3)$$

where:

- α_1 – the angle between the direction of incident light and the normal to the boundary surface;
- α_2 – the similarly, on the other side of boundary surface;
- V_1, V_2 – the speed of light in the medium 1 and 2, respectively.

Simplifying the problem to the two areas (1 and 2) with the temperatures T_1 and T_2 , where $T_1 > T_2$, in the area 1 the gas density is lower and consequently the speed of light is greater than in the area 2, so the angle $\alpha_1 > \alpha_2$ (Fig. 5.3). In this situation, the rays emitted from the plate areas hidden behind the horizon of the edge falling on the boundary surface of these areas will be broken down

and may hit the lens of the camera – hence an aura appears – in fact, a mirage image of the plate surface. In reality, there is a continuous change in the density of the gas, so the rays will run along the convex arc.

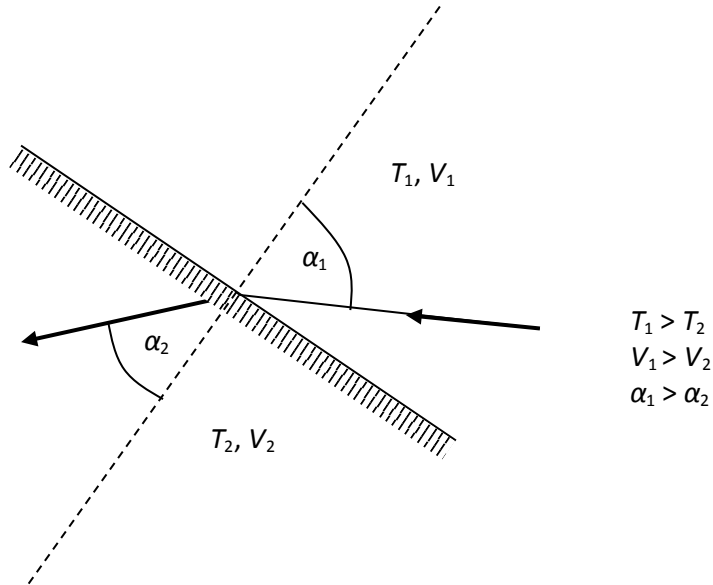


Fig. 5.3. The transition of light rays through the borders of two media with different temperatures (Strzecha et al., 2012)

This hypothesis is further supported by the fact that the aura on the drop contour is very thin. Continuing the argument – this results from the drop curvature – the mechanism described directs the radiation to the camera only from a narrow band adjacent to the contour just beyond the horizon.

5.1. Correction of the “Gas lens” Effects

The full correction of the phenomena described associated with the flow of protective gas in the furnace chamber is not possible. Among them, a particularly strong impact on the quality of the acquired images has the effect of "gas lens". Measurement system developers have concluded that the most effective and the simplest method of correction is to develop and implement an auto-focus algorithm, which will evaluate focus (contrast) of the image during the experiment and, if necessary, carry out complex correction by the appropriate positioning of the camera.

The proposed algorithm is passive, based on the contrast measurement. Its operation can be divided into four basic stages.

Stage 1: Definition of the auto-focus point mesh

The mesh of auto-focus points defines which image pixels will be considered in determining its focus. The density of the mesh should be chosen to minimize the computational cost, without significantly affecting the quality of processing. The orientation and location of points depend on the edge types found in the image. In the THERMO-WET system two meshes are used:

- with the horizontal auto-focus points, making an assessment of the vertical edges contrast possible (specimen);
- with the vertical auto-focus points, making an assessment of the horizontal edges contrast possible (measurement table).

The proposed mesh of horizontally oriented auto-focus points is presented in Fig. 5.4.

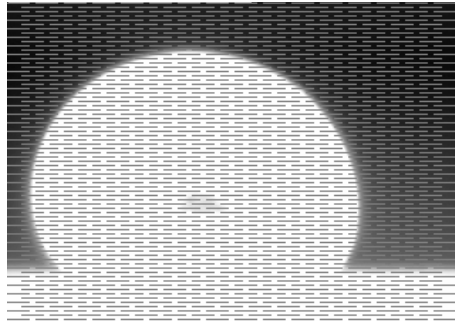


Fig. 5.4. The mesh of horizontal oriented auto-focus points

Stage 2: Selecting auto-focus points intersecting edges

The second stage of the algorithm is designed to identify the auto-focus points intersected by the edges in the digital image. The following operations are carried out sequentially:

- for all the pixels in the image corresponding to the auto-focus points the gradient is evaluated;
- within each auto-focus point, a pixel with the maximum value of gradient is selected;

- auto-focus points relevant to the assessment of image sharpness are selected; the selection is made on the basis of comparison of the maximum gradient value within an auto-focus point with the experimentally determined threshold (Fig. 5.5).

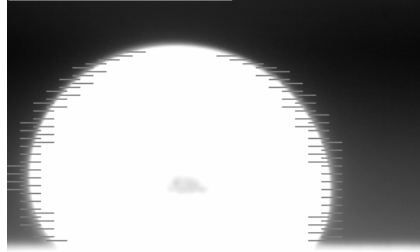


Fig. 5.5. The result of the second stage of auto-focus algorithm for the mesh of horizontal auto-focus points

Stage 3: Contrast ratio determination

In the third stage the contrast ratio of the analyzed image is determined. It is calculated as the average value of the maximum gradient of auto-focus points selected in the second stage. The designated contrast ratio is a measure defining the edge sharpness in the image.

The results of the algorithm described for a series of images obtained on the THERMO-WET system are shown in Fig. 5.6. Image B is an image with an optimal contrast, image A was acquired for the minimum distance between the specimen and the camera, and image of C for the maximum distance. Images A, B and C are shown in Fig. 5.7.



Fig. 5.6. Contrast ratio as a function of distance of the camera from the specimen: A - minimum distance, B - optimal contrast, C - maximum distance

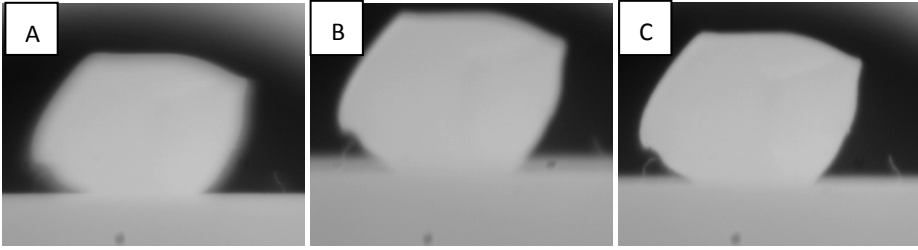


Fig. 5.7. Images obtained during the experimental verification of auto-focus algorithm: A - minimum distance, B - optimal contrast, C - maximum distance

Stage 4: Camera positioning

The final stage of the algorithm is to correct the position of the camera. It is carried out only when the value of the contrast ratio decreases by more than the assumed threshold. For two images obtained for adjacent camera positions, contrast values are compared and, on this basis, the direction of movement of the camera is determined. The camera is moved until the maximum value of contrast ratio is acquired.

Critical to the quality of the results obtained using the presented algorithm is an adequate selection of a gradient threshold under which the choice of auto-focus points for further analysis is made. Figure 5.8 shows the experimental results for two different values of the threshold. It is clear that if its value is too low, the distinguishing of the contrast in the sequence of images is weaker.

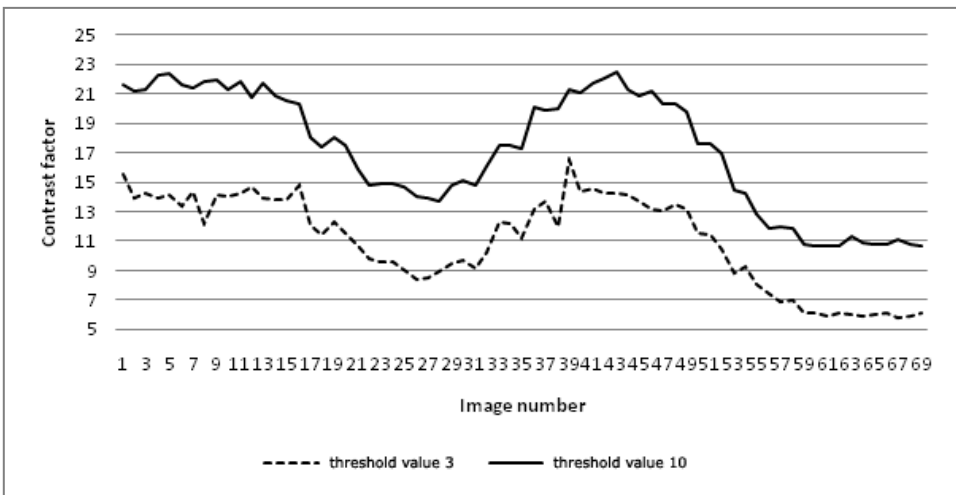


Fig. 5.8. Contrast ratio as a function of distance of the camera from a specimen for two different values of gradient threshold

The auto-focus algorithm was tested for two different methods of determining the values of gradients, using two and four-point derivative. The graph in Figure 5.9 illustrates the results obtained. Both methods give similar results. Consequently, the final version of the algorithm uses a 2-point derivative as computationally less expensive.

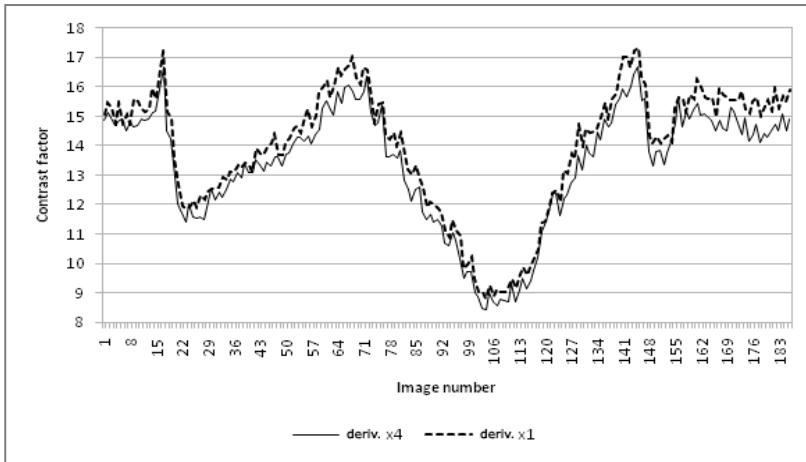


Fig. 5.9. Contrast ratio as a function of distance of the camera from a specimen for two different methods of determining the value of the gradient

The problem to be solved was the rapid change in the value of the contrast ratio for neighboring images. Simple filtration obtained by averaging the contrast factor values for the four images obtained for neighboring camera positions proved to be an effective solution. The results are shown in Figure 5.10.

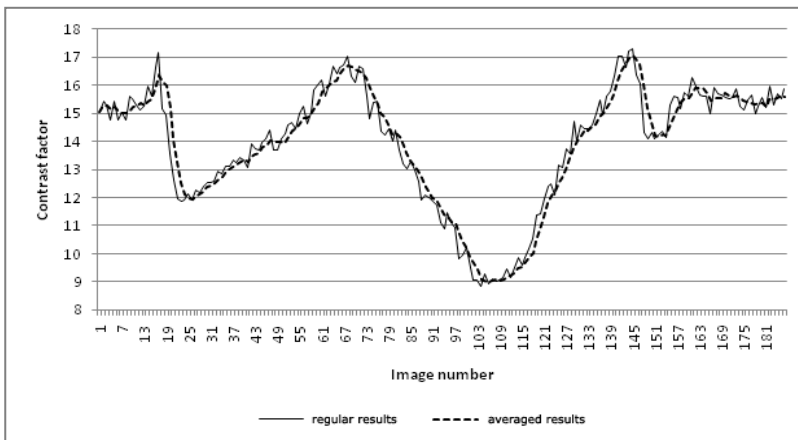


Fig. 5.10. Contrast ratio as a function of distance of the camera from a specimen with and without averaging

The proposed auto-focus algorithm allows such camera positioning during the measurement experiment that images obtained in the entire temperature range are characterized by a similar, high quality, parameters, independent of the actual "gas lens".

5.2. Aura Removal

Another factor resulting from the specificity of measurements performed by the THERMO-WET system is the aura effect. A specimen heated to a high temperature emits light in the visible part of the spectrum. The illumination causes the saturation of the CCD chip photosensitive elements. In order to diminish mid-infrared (thermal) radiation, infrared filters are used. However, it is impossible to completely eliminate the aura i.e. a glow that forms around the specimen.

Most image segmentation algorithms join the aura with the object, which increases specimen dimensions. Moreover, information about the specimen shape and the upper edge of the base plate localization is lost. Therefore, in order to ensure a high quality of image segmentation and the precision of surface property determination, the aura should be removed from the analyzed scene before the segmentation.

The proposed algorithm of aura removal uses Sobel gradient operators to find areas of an approximately constant intensity value. They are excluded from further analysis. Areas of appropriately high gradient are regarded as an aura and left unchanged. A block diagram of the proposed algorithm of the aura removal algorithm is presented in Figure 5.11. After the aura is extracted, it is simply subtracted from the analyzed image. The image is then subjected to the segmentation process.

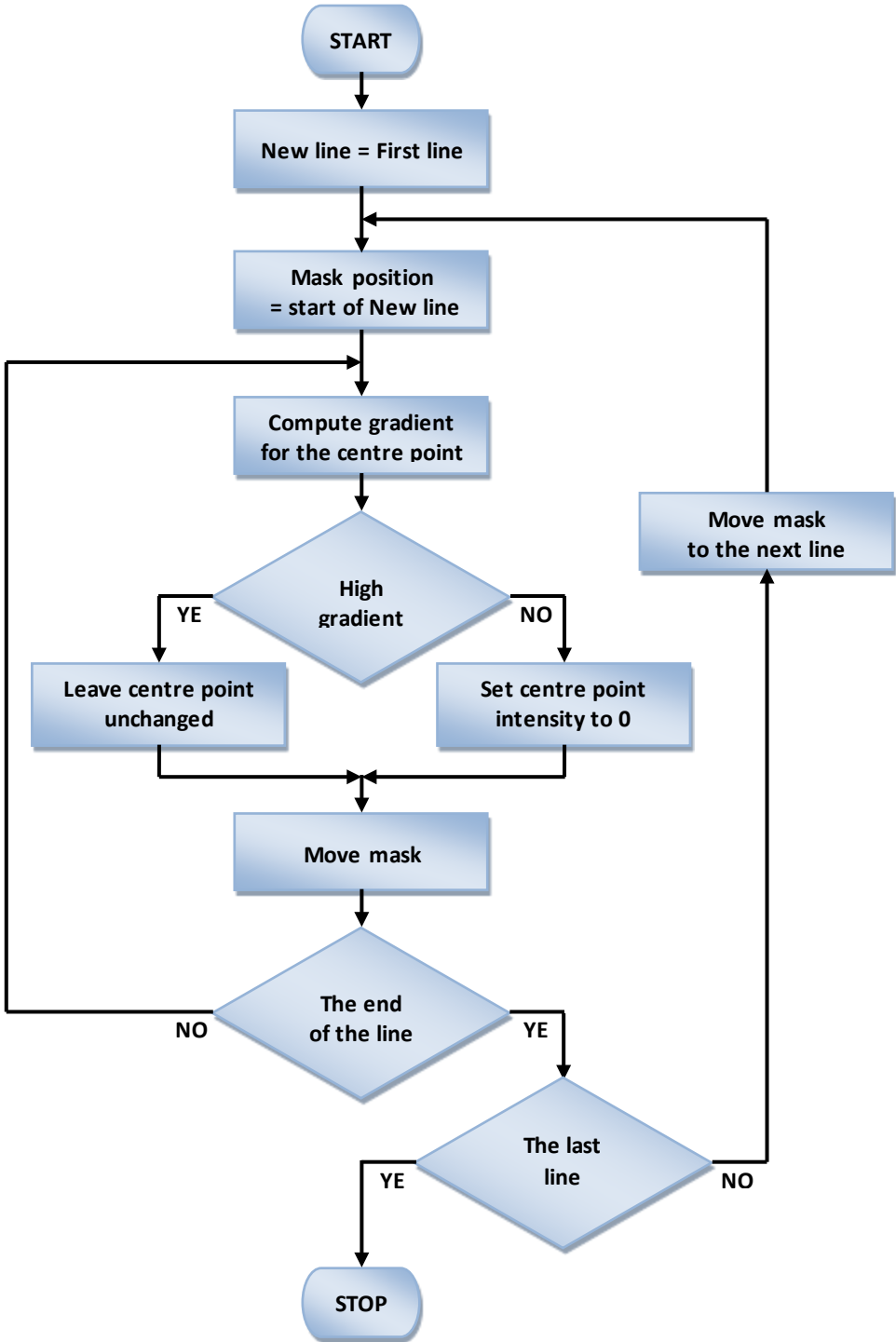


Fig. 5.11. Block diagram of aura extraction algorithm

The results of applying the aura removal algorithm to an exemplary image are presented in Fig. 5.12. Fig. 5.12a shows the original image (copper at 1239°C). The results of segmentation of the original image are presented in Fig. 5.12b. In Fig. 5.12c the aura-removed image after segmentation can be seen. The horizontal line indicates an approximate localization of the upper edge of the base plate.

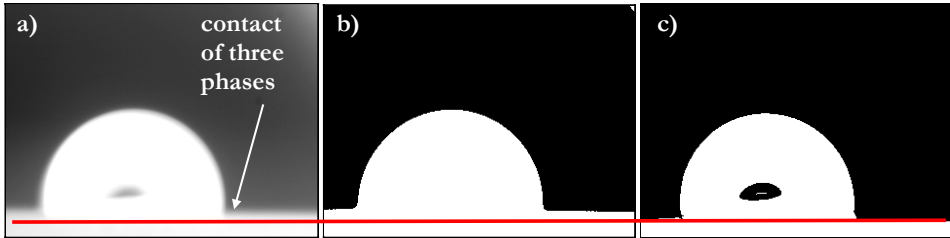


Fig. 5.12. Influence of aura removal process on image segmentation quality;
a) original image, copper, 1239°C; b) original image after segmentation;
c) aura-removed image after segmentation

In the case of no aura-removed image after segmentation, the displacement of the base line can easily be seen (Fig. 5.12b). Moreover, important information about the specimen shape and the upper edge of base plate localization (especially in contact of three phases) is lost. It can easily be seen that if image segmentation is preceded by aura removal, the quality of specimen shape determination is significantly improved (Fig. 5.12c). The edges of objects after segmentation are smooth and free from defects. Moreover, significant details of the specimen shape are extracted. The contours obtained provide good estimates of the contours of objects in the original image. The upper edge of the base plate is clear and well defined. Its localization matches the original image. The images obtained can be then successfully used for the further quantitative analysis.

6. Segmentation

One of the most difficult and the most important problems of image processing is segmentation. The purpose of segmentation is to divide a set of points on the digital image to disjoint subsets that meet certain criteria for homogeneity (e.g. color, brightness, texture). Each of these subsets has a specific meaning in relation to the characteristics of the observed scene. Although a wide range of different segmentation techniques is known (Fu et al., 1981; Haralick and Shapiro, 1985; Reed and du Buf, 1993; Li and Gray, 2000; Suri et al., 2002; Yoo, 2004; Nieniewski, 2005; Suri et al., 2005; Sun, 2006; Zhang, 2006), there is no general theory of segmentation.

After a detailed theoretical analysis and experimental verification of various groups of segmentation algorithms, the main assumptions for the segmentation in THERMO-WET system were made (Koszmider and Strzecha, 2008; Strzecha and Koszmider, 2008):

- developed image segmentation algorithms will be based on edge detection using a gradient filter with dynamically selectable masks;
- algorithms will provide high-quality treatment necessary in measuring systems, understood as giving a precise shape and dimensions of objects in the scene.

6.1. Algorithm for Fast Specimen Localization

The task of the algorithm is to provide information on the approximate location of the specimen within the analyzed scene with the minimum possible calculation effort. The resulting location of the sample is described by five location points (Fig. 6.1):

- A, E – the upper edge of the tray table;
- B, D – the left and the right extreme point of the sample;
- C – the top of the drop.

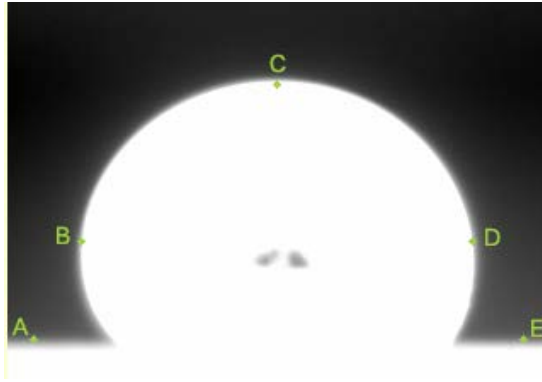


Fig. 6.1. Specimen location points

The task of the first stage of the fast specimen localization algorithm is to determine the location of the upper edge of the measurement table (A, E). For this purpose, from all points of the columns outermost of $1/20$ of the width of the image from its left and right boundary, the pair of pixels distant from each other by the number of pixels representing 2% of the image height, for which the difference of brightness is the greatest, is determined. The greater brightness of the determined pixels will be the brightness value with which the specimen will be identified in the next stage of the algorithm (Fig. 6.2).

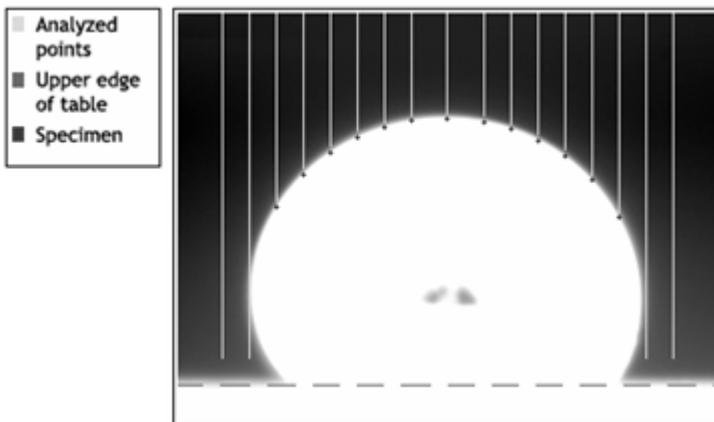


Fig. 6.2. Idea of fast drop localization algorithm

In the second stage, points D, C and B are searched for in subsequent columns between the first and 15th pixel row above the upper edge of the measurement table. Depending on the point searched for, the algorithm uses one of the following criteria:

- point D: the first point with three following points having the brightness higher or equal to the specimen brightness found in the first phase of the algorithm;
- point C: the highest point found with the same criteria as point D, but belonging to a different column;
- point B: the last point found with the same criteria as point D.

If any of the location points are not found, the algorithm assumes that the image does not represent the specimen or its quality is insufficient for the purposes of further analysis.

The low computational complexity of the discussed algorithm results from the limitation of the number of analyzed points to only 5% of all the pixels. The algorithm examines only the columns separated by a distance equal to 1/20 of the width of the image.

6.2. Edge Detection with Dynamic Selection of Filtration Masks

The algorithm described below is a modified gradient filter which uses directional Sobel masks for 4 base gradient vector directions (Fig. 6.3).

Based on the drop localization points the gradient filtration algorithm specifies areas of drop fragments, for which the gradient vector directions and the axis of ordinates create approximate angles of 0° , 45° , 90° or 135° .

For such defined areas, algorithms select the most appropriate masks (Fig. 6.4):

- the area containing point C: both cross line and horizontal;
- the areas containing points B, D: both cross line and vertical;
- the areas below points A, E: horizontal line mask;
- the remaining areas: both cross line masks.

The edge extraction relies upon the collecting points with the highest value of gradient for the local gradient direction.

<i>Cross line masks [3x3]</i>					
2	1	0	0	1	2
1	0	-1	-1	0	1
0	-1	-2	-2	-1	0
<i>Horizontal and vertical line masks [3x3]</i>					
1	2	1	-1	0	1
0	0	0	-2	0	2
-1	-2	-1	-1	0	1

Fig. 6.3. Sobel mask for four basic directions of the vector gradient

The presented algorithm is characterized by a higher precision of the edge localization by matching the type of masks used for the shape of the object in the analyzed scene. Its computational cost is significantly lower than the classical Sobel method due to the reduction in the number of masks, and the reduction of the number of pixels for which the convolution is performed.

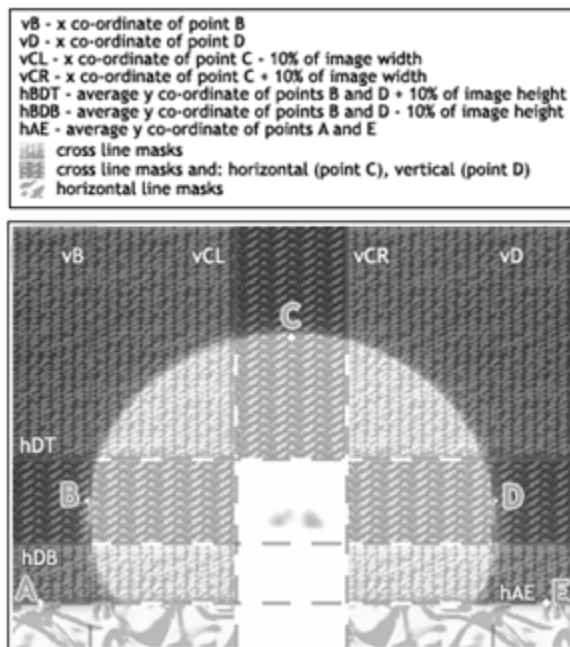


Fig. 6.4. The use of gradient filter masks in different drop areas

6.3. Contour Tracing

The last stage of segmentation is responsible for extracting the object from the pre-processed image and presenting it as a list of pixels forming the edge outlining the specimen along with the table. A further analysis of such a list will be possible only if the points it contains will form a continuous edge which:

- is the width of one pixel;
- consists of the points with the maximum of two n-neighbors;
- begins in the first and ends on the last column of the image.

The convolution of an image with a point detection mask gives, as a result, a map of edge points (Fig. 15.28). These points will form a continuous one pixel wide edge if the points in the neighborhood of two consecutive n-neighbors of the concerned edge map element will be deleted. Thus, the obtained list of points represents the binary form of the one-pixel-wide edge.

<i>Point detection mask</i>	<i>N-neighbor detection mask</i>																		
<table border="1"><tr><td>-1</td><td>-1</td><td>-1</td></tr><tr><td>-1</td><td>8</td><td>-1</td></tr><tr><td>-1</td><td>-1</td><td>-1</td></tr></table>	-1	-1	-1	-1	8	-1	-1	-1	-1	<table border="1"><tr><td>0</td><td>-1</td><td>0</td></tr><tr><td>-1</td><td>0</td><td>-1</td></tr><tr><td>0</td><td>-1</td><td>0</td></tr></table>	0	-1	0	-1	0	-1	0	-1	0
-1	-1	-1																	
-1	8	-1																	
-1	-1	-1																	
0	-1	0																	
-1	0	-1																	
0	-1	0																	

Fig. 6.5. Point and n-neighbor detection masks

To verify the continuity of the determined edge simplified contour tracking algorithm based on the analysis of the nearest neighborhood of edge points was used. This algorithm also checks whether the starting point of the edge is in the first, and the final in the last column of the image.

The contour tracking process begins by finding the edge point located in the first column of the image, which initializes the major loop of the algorithm. In this loop n-neighborhood of the current point is tested. Depending on the result of the convolution of the n-neighbor detection mask (Fig. 6.5) with a given point of the image, one of the following actions is taken:

- 1 n-neighbor – deletes all the points added from the last node from the list (more than two n-neighbors) and re-examines its n-neighborhood without the previously considered n-neighbors;
- 2 n-neighbors – considers the n-neighbor, which is not included in the resulting list, as the next point of the edge;
- 3 or 4 n-neighbors – marks the point currently under consideration as a node, and classifies the first encountered n-neighbor, which is not included in the resulting list, as the next edge point, which does not contain a list of the resulting.

The algorithm terminates when the currently considered point belongs to the last column of the image and has only one n-neighbor. However, if the point having one n-neighbor does not belong to the last column of the image, and all n-neighbors of the last node have been processed, the algorithm aborts, indicating that the edge meeting the initial assumption has not been found. Such an image cannot be sent for further analysis.

The final result of the segmentation algorithms developed specifically for the THERMO-WET system is shown in Fig. 6.6.

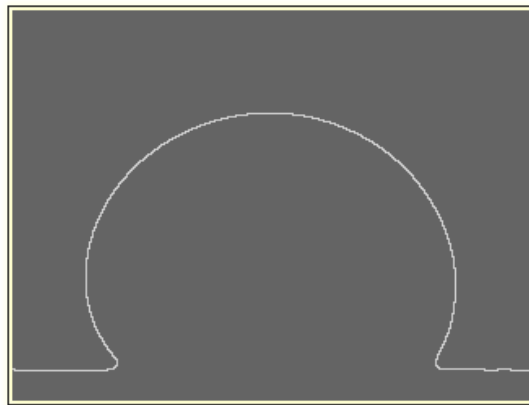


Fig. 6.6. The final result of the segmentation process

6.4. Profile Correction at the Contact Point of the Three Phases

In the THERMO-WET system the proper determination of contact angles is hindered by a number of phenomena related to the measurements at high temperatures, the most significant of which are:

- an aura;
- a small depth of field of the optical system;
- physicochemical phenomena occurring in the three phases of contact.

The actual shape of the profile of the specimen resulting from the above mentioned phenomena is shown in Fig. 6.7. The deformation of the specimen profile is clearly visible around the contact point of the three phases.

In order to avoid the influence of the specimen profile deformation on measurement results there is a need to identify and skip deformation points in further calculations. This operation is performed for both the left and the right profile of the sample. The following operations are carried out sequentially:

- extending the set of the edge points of the specimen in such a way that the contact point of the three phases is not the utmost point;
- approximating the specimen with the fifth or sixth degree polynomial (depending on the shape of the sample) using an extended set of boundary points;
- defining the tangent to the curve approximating the profile of the specimen at the point of three phases contact.

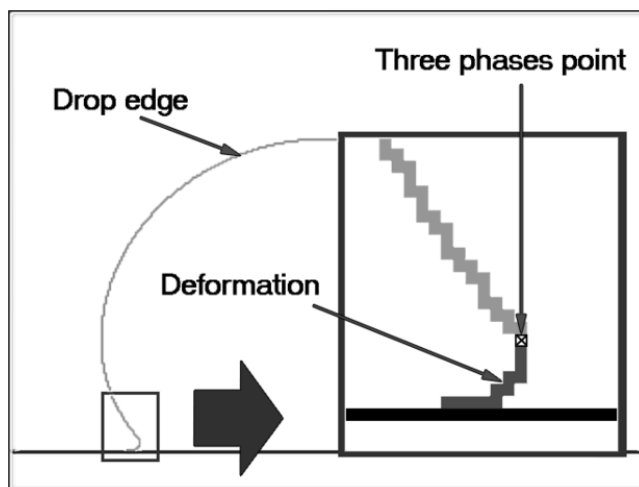


Fig. 6.7. The deformation of the specimen profile at the contact point of the three phases

The knowledge of the tangent to the profile of the specimen at the point of three phase contact allows one to determine contact angles on the basis of elementary mathematical relationships.

The algorithm of extending the set of the specimen edge points has a particular significance for the process of determining the contact angles. Its idea is illustrated in Fig. 6.8. For this purpose, first the specimen profile is approximated with a polynomial of the fifth or sixth degree (excluding points in the deformation), next, the tangent to the profile of the specimen at the point of three phase contact is determined. The resulting tangent becomes the axis of ordinates OY' in the local coordinate system with the origin at the three phase contact point.

Extending the set of profile points is simply determining points A' axially symmetric to axis OX' of the local coordinate systems. Points are added to the set of points above the point of three phase contact A .

Knowing the equations of lines along the axes OX' and OY' in the local coordinate system and the coordinates of point A in the global coordinate system, it is possible to designate coordinates x' and y' as the distances from the axes OY' and OX' , respectively:

$$x' = \frac{|Ax + By + C|}{\sqrt{A^2 + B^2}}; \quad (6.1)$$

$$y' = \frac{\left| \frac{1}{A}x + By + C \right|}{\sqrt{A^2 + B^2}}. \quad (6.2)$$

The determination of extra points is equivalent to the solution of equations (6.1) and (6.2) for the local variables x' and $-y'$.

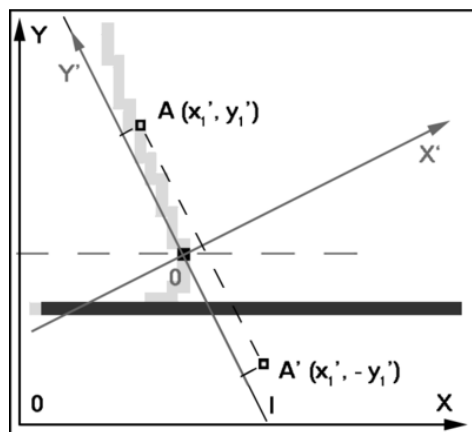


Fig. 6.8. Determination of extra points of the specimen profile

The results of contact angle determination in an exemplary image of a low carbon steel specimen at a temperature of 1500°C are shown in Fig. 6.9. Fig. 6.9a shows the original image obtained during the measurement process. In Fig. 6.9b contact angle determination results obtained using the original specimen profile are shown. Finally, Fig. 6.9c presents the results obtained after extending the specimen profile using the proposed method. It is clearly visible that in the case of the considered drop of molten steel, contact angles are below 90°, while ones determined from the original profile are above 90°. Extending the specimen profile using the method described allows one to obtain results with values lower than 90°.

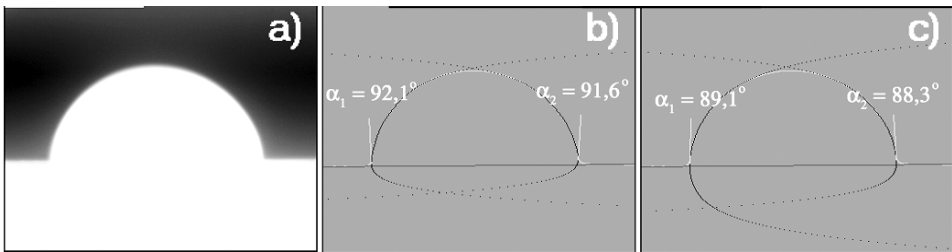


Fig. 6.9. Results of contact angle determination in exemplary image of the low carbon steel specimen at the temperature 1500°C: a) original image; b) results obtained using the original profile; c) results obtained after extending the specimen profile using the presented method

In Fig. 6.10 the results of contact angle determination in images of copper at temperatures of 1050°C-1600°C are shown. The results obtained using the old and the new methods are compared with the results obtained using ADSA (Cheng et al., 1990; Cheng and Neumann, 1992; del Rio and Neumann, 1997) approach used as a reference.

The old method for contact angle determination provides angles characterized by high deviation. Moreover, the determined values of contact angles are significantly smaller than the reference ones provided by ADSA. The introduced method for contact angle determination significantly improves the quality of the results obtained. The determined values are very close to the reference ones and are characterized by smaller deviation.

It should be underlined that the ADSA method used as a reference is characterized by high computational complexity. In addition, it requires a well-defined profile of the specimen, which is usually selected by the system operator.

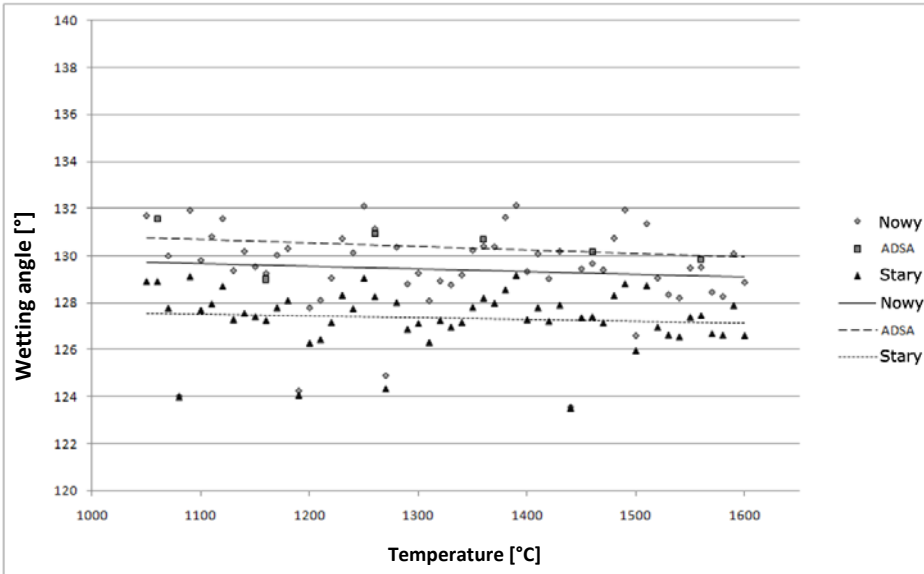


Fig. 6.10. Results of contact angle determination between Al₂O₃ and copper at temperature 1050°C-1600°C

6.5. Subpixel Edge Detection

Research presented in this chapter were carried out under the project no. N N519 403037 and were described in detail along with their continuing in (Fabijańska, 2012).

In the system considered the precise determination of an object dimension is crucial for the accuracy of measurements. However, due to very intense thermal radiation and aura phenomena, edge detection performed with the traditional accuracy (Davis, 1975; Marr and Hildreth, 1980; Haralick, 1982; Canny, 1986; Bergholm, 1987; Deriche, 1987; Ziou and Tabbone, 1998; Basu, 2002; Senthilkumaran and Rajesh, 2009) fails to properly define the shape of objects present on the scene. The edge between the object and the background is supposed to be located inside the aura. However, its exact position is not clearly defined. Well-established (derivative-based) methods for edge detection produce different results when applied to the same image. Most commonly, the aura is connected with the object, which increases object dimensions. This, in turn, influences the determined values of surface tension which is calculated based on the characteristic dimensions of the specimen.

Therefore, the method for improving the quality of edge detection was introduced. The approach proposed determines edges with sub-pixel accuracy and eliminates weaknesses of the traditional methods for edge detection (Hung and Ridd, 2002; Jivin and Rotman, 2008; Weng and Lu, 2009, Bauda et al, 2010).

The main concept of the proposed method is to create continuous functions out of the image derivative values provided by the popular approaches to edge detection. Specifically, the Sobel gradient detector is considered. The neighborhood of each coarse edge-pixel provided by the Sobel edge detector is examined in order to build continuous image derivatives in a given direction. The subpixel edge position is indicated by the maximum of the created (i.e. continuous) function.

The introduced approach operates in two main stages, namely:

- the determination of the coarse edge;
- the determination of the subpixel edge.

Sobel masks (the horizontal h_x and the vertical h_y) are applied in order to determine the coarse edge. The input image L is convolved with each mask separately in accordance with Equations (6.3) and (6.4). These operations produce images of gradient in horizontal and vertical directions, respectively.

$$|\nabla L_x| \equiv |h_x \otimes L|; \quad (6.3)$$

$$|\nabla L_y| \equiv |h_y \otimes L|; \quad (6.4)$$

where:

\otimes denotes the convolution.

Next, local intensity maxima are determined along the non-zero pixels of the gradient images ∇L_x and ∇L_y . In the case of image ∇L_x , the search is performed in a horizontal direction and two local maxima (for the left and the right side of the image) are determined in each row. This operation is expressed by Equations (6.5-6.8). Image ∇L_y is searched in a vertical direction and locates one maximum in each column (see Eq. (6.8)).

$$\partial L_x = \partial L_{xl} \cup \partial L_{xr}; \quad (6.5)$$

where:

$$\partial L_{xl}(x, y) = \begin{cases} 1 & \text{for } \nabla L(x, y) = \max_{1 \leq x < N/2} (\nabla L(x, y)); \\ 0 & \text{otherwise} \end{cases}; \quad (6.6)$$

$$\partial L_{xr}(x, y) = \begin{cases} 1 & \text{for } \nabla L(x, y) = \max_{N/2 \leq x \leq N} (\nabla L(x, y)); \\ 0 & \text{otherwise} \end{cases}; \quad (6.7)$$

$$\partial L_y(x, y) = \begin{cases} 1 & \text{for } \nabla L(x, y) = \max_{1 \leq y \leq M} (\nabla L(x, y)); \\ 0 & \text{otherwise} \end{cases}; \quad (6.8)$$

where:

N, M – horizontal and vertical image resolution.

The operations described above produce binary images of one-pixel width coarse edges in horizontal and vertical directions. These binary images are input data for refining the edge location performed in the next step.

Successive steps of the coarse edge detection applied to the exemplary image of heat-emitting steel cylinder at 1020°C are presented in Figure 6.11. In particular, Figure 6.11a shows an exemplary image obtained with 8-bit grayscale resolution and spatial resolution $M \times N$ of 240×320 pixels. The edges in the exemplary image are significantly blurred due to intense thermal radiation emitted by the steel cylinder. In Figures 6.11b and 6.11c images of gradient in horizontal and vertical directions are shown. Figures 6.11d and 6.11e present the corresponding edges in vertical and horizontal directions. In Figure 6.11f a complete coarse edge composed from horizontal and vertical components can be seen. Negatives are shown in order to improve the readability of images.

It can easily be seen (Fig. 6.11) that in the case of significantly blurred edges their coarse representation is irregular and discontinuous. There are significant deviations from the main direction of the edge. Therefore, in the next step the coarse location of edges is refined using numerical and mathematical methods.

After the coarse edge is found, its location is refined to subpixel position. The accurate location of the edge is approximated using polynomials. Especially, least-square approximation is used. It aims at modeling continuous functions out of the discrete gradient values in the neighborhood of pixels

qualified to the coarse edge. The linear neighborhood in the gradient direction is considered; s pixels on each side of the coarse edge pixel are used. The coordinates of the maximum of the approximated gradient function determine the edge location with sub-pixel accuracy. The main idea of refining the edge location to a sub-pixel level is sketched in Figure 6.12.

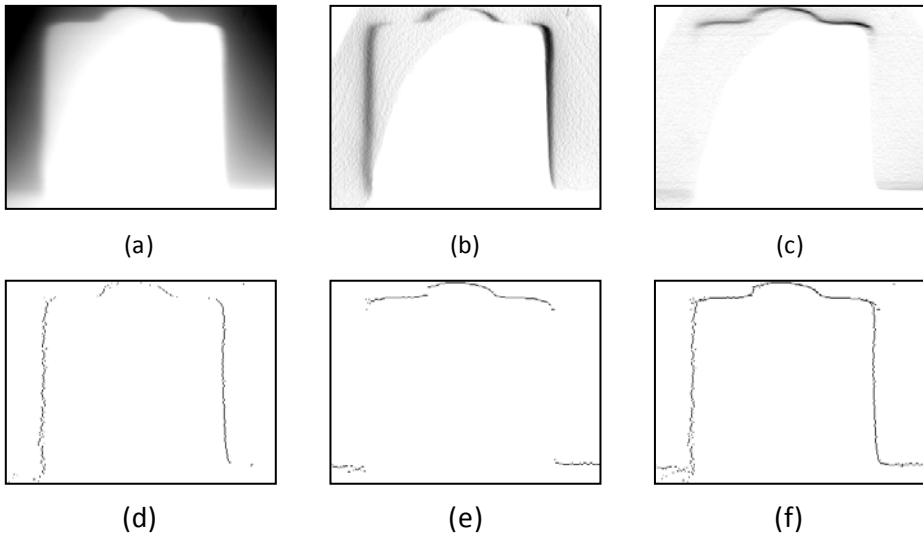


Fig. 6.11. Successive steps of coarse edge determination; (a) exemplary image of steel cylinder at 1020°C; (b) horizontal gradient; (c) vertical gradient; (d) coarse vertical edge; (e) coarse horizontal edge; (f) complete coarse edge composed from horizontal and vertical component

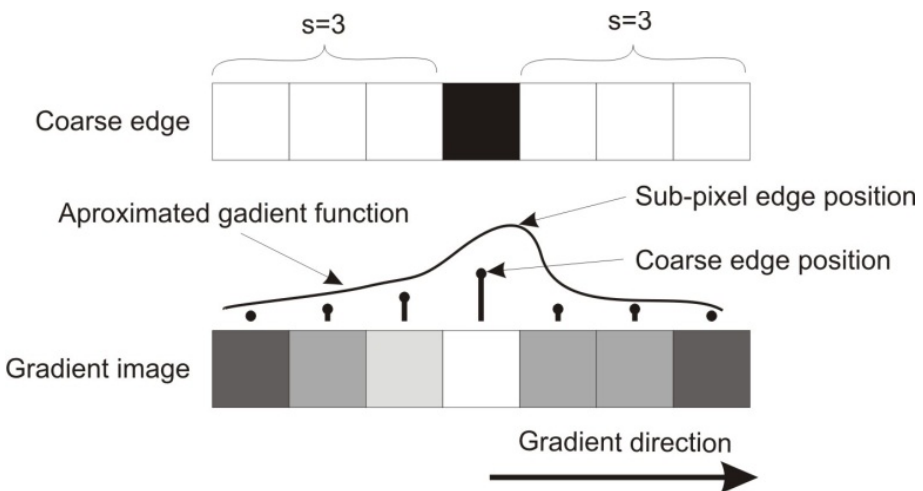


Fig. 6.12. The idea of sub-pixel edge detection using the proposed method

The experimental results proved that the best (i.e. most regular) edges are obtained when a second-grade polynomial is used. Regardless of the neighborhood size, approximation using Trinomial Square provides the most stable approximation results.

The results of edge detection with sub-pixel accuracy in the images of heat-emitting specimens of metals and alloys are presented in Figure 6.13. In particular, Figure 6.13a presents the input image, Figure 6.13b corresponds with the edge detected with pixel accuracy using Sobel gradient masks and in Figure 6.13c the sub-pixel edge is presented. Finally, the comparison of the input image and the detected (i.e. sub-pixel) edge is given in Figure 6.13d. The input images are denoted by numbers 1–4 and present low carbon steel at 1200°C, low carbon steel at 1000°C, silver at 1200°C, and low carbon steel at 880°C, respectively. Due to the limitations of the digital raster, the pixel position in the image of the refined edge was rounded to the closest integer value.

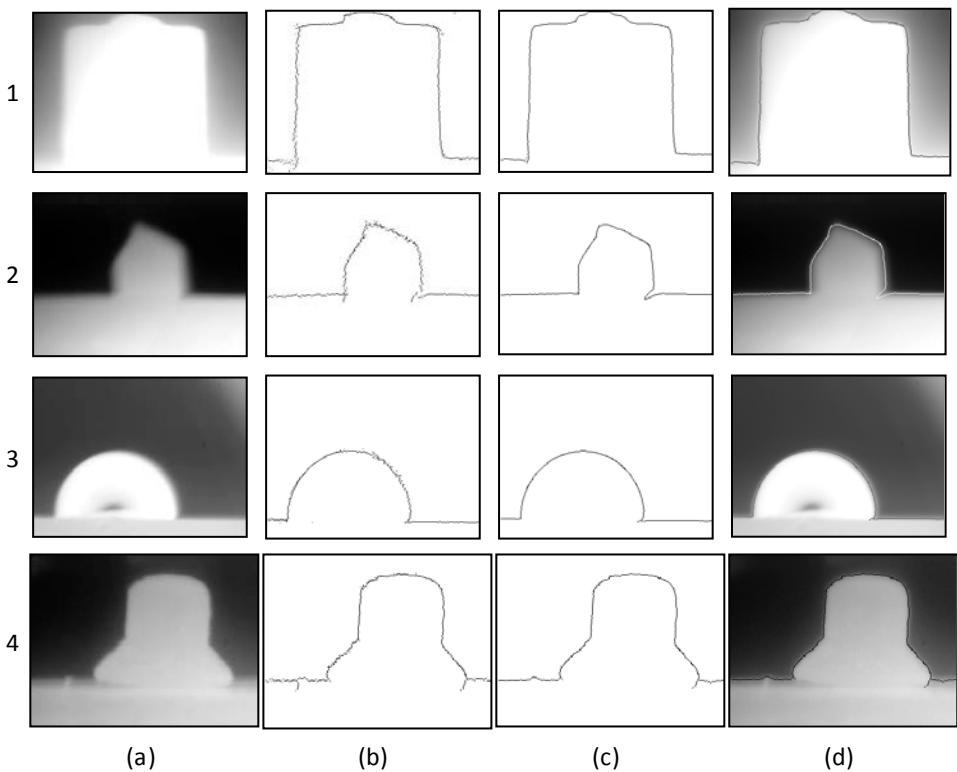


Fig. 6.13. Results of edge detection with the sub-pixel accuracy; (a) original image; (b) edge detected with pixel accuracy; (c) sub-pixel edge; 1 – low carbon steel, 1200°C; 2 – low carbon steel I, 1000°C; 3 – silver, 1200°C; 4 – low carbon steel, 880°C

The results of applying the method proposed to heat-emitting images prove that sub-pixel processing significantly improves the quality of edge detection. The refined edges are continuous and much more regular than those provided by Sobel gradient masks. The more blurred is the edge, the more significant the difference.

The method proposed was developed for images of heat-emitting objects. However, it can be successfully applied in a wide spectrum of applications.

7. Conclusions

In a large number of applications, modern industrial measuring instruments are built on the basis of vision systems the task of which is the acquisition, analysis and processing of images leading to a quantitative description of the scene recorded. The accuracy of this type of measuring instruments depends, to a considerable extent, on the quality of image processing and analysis algorithms implemented in them. Requirements imposed on measuring apparatus cause the development and implementation of this kind of algorithms by scientists to be a particularly difficult and, at the same time, extraordinarily interesting challenge. This type of algorithms can be divided into three groups, especially important from the viewpoint of issues of quantitative image analysis systems:

1. Algorithms of preliminary processing of images, the purpose of which is, above all, the correction of noise introduced to the signal acquired by all the vision system elements (e.g. lens or video sensor), and the conditions in which a scene is recorded (e.g. lighting or the atmosphere).
2. Algorithms of image segmentation constituting one of the most difficult and, at the same time, the most important problems that require solving during the design of quantitative image analysis systems. Their task is to divide the image into disjunctive subsets satisfying certain criteria of uniformity (e.g. color, brightness level or texture). The segmentation result should allow one to perform possibly the most accurate measurement of geometrical features of objects in the scene at the smallest possible calculation cost.
3. Algorithms of image analysis understood as a process of formation of a quantitative description of features of the scene recorded, obtained from calculations, in accordance with the scene model assumed and the optical system. The model should account for the relationships between the distribution of light intensity radiation of the scene points containing objects of the class under consideration and the digital image brightness. In addition, it should take into consideration all the side effects caused by the imperfection of the camera and electronics in the image analysis system, which can have a negative impact on the accuracy of measurement of the image features.

In the present book a number of new original algorithms of image processing and analysis have been presented, which can be used in industrial measuring systems constructed on the basis of vision subsystems. All the algorithms presented have been designed with a view to being used on a THERMO-WET measuring stand (Chapters 2 and 3).

The first group of algorithms presented aims at the improvement of quality of the images acquired (Chapter 4). The measurement of surface properties of metals in the THERMO-WET system requires the precise determination of geometrical properties of liquid specimens of metals. The accurate measurement of these parameters is considerably hindered by the errors caused by all the elements of the vision system. This problem can be solved by the development and use of specialized algorithms compensating a negative effect of the vision system components and the advanced switching filters. The known algorithms of the preliminary processing cause a loss of part of the significant image information, which – in most applications of image quantitative analysis – is unacceptable. The distinctness of the proposed approach towards preliminary image processing consists in the treatment of image noise in a causative manner. Knowing the character of noise introduced by the vision system and those resulting from measurement, it turned out that it was possible to construct such preliminary processing algorithms that remove only a minimal part of image information. Due to such an approach it is possible to prevent the loss of information particularly important from the point of view of quantitative image analysis processes.

The second group of algorithms encompasses algorithms of correction of errors introduced into the image by the flow of gasses (Chapter 5). The measurement of surface properties of metals in the THERMO-WET system requires the use of a protective atmosphere. The flow of gas at a high temperature causes a number of phenomena that have a negative effect on the precise localization of the specimen edges of the material under investigation, first of all, the “gas lens” and the “aura”. An attempt to solve this problem was undertaken by developing specialized algorithms compensating the effect of the aforementioned phenomena.

One of the most difficult and, at the same time, the most important problems of image processing is segmentation (Chapter 6). It is the quality of segmentation

algorithms that the accuracy of further analysis of the image depends on. The image segmentation algorithms developed were based on the detection of edges using gradient filters with a dynamically selected mask. They ensure a high quality of processing, necessary in measurements systems, understood as the precise rendering of the shape and size of objects of the scene in the resulting image. Segmentation quality has a critical effect on the accuracy of measurement of geometrical parameters liquid metal specimens in the THERMO-WET system. The specificity of images of objects at high temperatures causes the segmentation process to be particularly difficult, and requires using specialized, dedicated algorithms. The algorithms developed aim at improving segmentation quality and thereby allow for possibly accurate representation of the specimen edge in the resulting image, especially in the vicinity of contact points of the three phases.

Attempts at using subpixel methods of edge localization in industrial measuring systems are rare. Their adaptation and implementation in a measuring station of surface tension and wetting angles was the first such attempt, and the results obtained fully confirmed their usefulness in applications of this type.

All the algorithms developed were implemented in the THERMO-WET measuring system of surface tension and wetting angles. In addition, a large number of labor-consuming measurement experiments were carried out, aimed at the experimental verification of the algorithms developed, placing particular emphasis on the accuracy of localization and measurement of geometrical parameters of the specimen of the material under investigation as those having a critical impact on the quality of the results obtained.

The use of the above-mentioned methods in the THERMO-WET measuring system allowed for obtaining distinct improvement of the quality of images acquired and increased the accuracy and reproducibility of measurements of surface properties.

It should be stressed that there is a considerable diversity between the development of the theory of processing and analysis of images and their practical applications for automated physical-chemical quantities. The Author hopes that the research discussed has, at least to a certain extent, contributed to filling this gap.

Bibliography

- Abreu E., Lightstone M., Mitra S.K., Arakawa K. (1996) A New Efficient Approach for the Removal of Impulse Noise from Highly Corrupted Images. *IEEE Transactions on Image Processing*, Vol. 5, No. 6, pp. 1012-1025.
- Acharya T., Ajoy K. (2005) *Image Processing: Principles and Application*. John Wiley & Sons.
- Adamson A.W., Gast A.P. (1997) *Physical Chemistry of Surfaces*. Wiley-Interscience, New York.
- Alajlan N., Jernigan E. (2004) An Effective Detail Preserving Filter for Impulse Noise Removal. *Image Analysis and Recognition, Lecture Notes in Computer Science*, Vol. 3211, pp. 139-146.
- Anastasiadis S.H., Chen J.K, Koberstein J.T, Siegel A.F., Sohn J.E., Emerson J. A. (1987) The Determination of Interfacial Tension by Video Image Processing of Pendant Fluid Drops. *Journal of Colloid and Interface Science*, Vol. 119, pp. 55-66.
- Atae-Allah C., Cabreizo-Vilchez M., Gomez-Lopera J.F., Holgado-Terriza J.A., Roman-Roldan R., Luque-Escamilla P.L. (2001) Measurement of Surface Tension and Contact Angle Using Entropic Edge Detection. *Measurement Science and Technology*, Vol. 12, No. 3, pp. 288-298.
- Awcock G.W., Thomas R. (1995) *Applied Image Processing*. McGraw Hill, New York.
- Bachevsky R.S., Naidich Y.V., Grygorenko M.F., Dostojny V.A. (1994) Evaluation of Errors in Automatic Image Analysis Determination of Sessile Drop Shapes. *Proc. Int. Conf. High Temperature Capillarity*, Smolenice Castle, pp. 254.258.
- Baglin J.E.E. (1988) *Thin Film Adhesion: New Possibilities for Interface Engineering*. *Material Science and Engineering*, Vol. B-1, pp. 1-7.
- Bąkała M. (2007) Wyznaczanie wybranych parametrów lutowności w wysokich temperaturach z wykorzystaniem metody płytkowej. PhD Thesis. Czestochowa University of Technology, Częstochowa, Poland (in Polish).
- Ballard D.H., Brown C.M. (1982) *Computer Vision*. Prentice Hall, New Jersey.

- Basu M. (2002) Gaussian-Based Edge-Detection Methods – A Survey. IEEE Transactions on Systems, Man, and Cybernetics, Part C: Applications and Reviews, Vol. 32, No. 3, pp. 252-260.
- Bauda I., Kufferb M., Pfeffer K., Sliuzasb R., Karuppananc S. (2010) Understanding Heterogeneity in Metropolitan India: The Added Value of Remote Sensing Data for Analyzing Sub-standard Residential Areas. International Journal of Applied Earth Observation and Geoinformation, Vol. 12, pp. 359-374.
- Bauer N. (2006) Guideline for Industrial Image Processing. Fraunhofer-Gesellschaft.
- Baxes G.A. (1994) Digital Image Processing: Principles and Applications. John Wiley & Sons, Los Altos.
- Bechstedt F. (2005) Principles of Surface Physics. Springer.
- Bergholm F. (1987) Edge Focusing. IEEE Transactions on Pattern Analysis and Machine Intelligence, Vol. 9, No. 6, pp. 726-741.
- Boncellet Ch. (2005) Image Noise Models. in Bovik A.: Handbook of Image and Video Processing. Academic Press.
- Booch G., Rumbaugh J., Jacobson I. (1998) The Unified Modeling Language User Guide. Addison-Wesley, Massachusetts.
- Bovik A.C. (2000) Handbook of Image And Video Processing. Academic Press.
- Bracco G., Holst B. (eds.) (2013) Surface Science Techniques. Springer-Verlag Berlin Heidelberg.
- Butt H.J., Graf K., Kappl M. (2003) Physics and Chemistry of Interfaces. John Wiley & Sons, Los Altos.
- Canny J. (1986) A Computational Approach to Edge Detection. IEEE Transactions on Pattern Analysis and Machine Intelligence, Vol. 8, pp. 679-714.
- Castleman K.R. (1996) Digital Image Processing. Prentice Hall, New Jersey.
- Chan R.H., Ho C.W., Nikolova M. (2005) Salt-and-Pepper Noise Removal by Median-Type Noise Detectors and Detail-Preserving Regularization. IEEE Transactions on Image Processing, Vol. 14, No. 10, pp. 1479-1485.
- Chan R.H., Hu C., Nikolova M. (2004) An Iterative Procedure for Removing Random-Valued Impulse Noise. IEEE Signal Processing Letters, Vol. 11, No. 12, pp. 921-924.

- Chellappa R. (1992) Digital Image Processing. IEEE Computer Society Press, New York.
- Cheng P., Li D., Boruvka L., Rotenberg Y., Neumann A.W. (1990) Automation of Axisymmetric Drop Shape Analysis for Measurement of Interfacial Tensions and Contact Angles. *Colloid Surfaces*, Vol. 43, pp. 151-167.
- Cheng P., Li D., Boruvka L., Rotenberg Y., Neumann A.W. (1990) Automation of axisymmetric drop shape analysis for measurements of interfacial tensions and contact angles. *Colloids and Surfaces*, Vol. 43, No. 2, pp. 151-167.
- Cheng P., Neumann, A.W. (1992) Computational evaluation of axisymmetric drop shape analysis-profile (ADSA-P). *Colloids and Surfaces*, Vol. 62, No. 4, pp. 297-305.
- Cwikel D., Zhao Q., Liu Ch., Su X., Marmur A. (2010) Comparing Contact Angle Measurements and Surface Tension Assessments of Solid Surfaces. *Langmuir*, Vol. 26, No. 19, pp. 15289-15294.
- Davies E.R. (2004) Machine Vision: Theory, Algorithms, Practicalities. Morgan Kaufmann.
- Davis L.S. (1975) A Survey of Edge Detection Techniques. *Computer Graphics and Image Processing*, Vol. 4, pp. 248-270.
- de Gennes P. (1985) Wetting: Statics and Dynamics. *Reviews of Modern Physics*, Vol. 57, No. 3, pp. 827-863.
- de Gennes P., Brochard-Wyart F., Quere D. (2003) Capillarity and Wetting Phenomena: Drops, Bubbles, Pearls, Waves. Springer-Verlag, Berlin.
- del Rio O.I., Neumann A.W. (1997) Axisymmetric Drop Shape Analysis: Computational Methods for the Measurement of Interfacial Properties from the Shape and Dimensions of Pendant and Sessile Drops. *Journal of Colloid and Interface Science*, Vol. 196, No. 2, pp. 136-147.
- Delannay F., Froyen L., Deruyttere A. (1987) The Wetting of Solids by Molten Metals and Its Relation to the Preparation of Metal-Matrix Composites. *Journal of Material Science*, Vol. 22, No. 1, pp. 1-16.
- Deriche R. (1987) Using Canny's Criteria to Derive a Recursively Implemented Optimal Edge Detector. *International Journal of Computer Vision*, Vol. 1, pp. 167-187.
- Deyev G.F., Deyev D.G. (2005) Surface Phenomena in Fusion Welding Processes. CRC Press.

- Dougherty E.R. (ed.) (1994) Digital Image Processing Methods. CRC Press.
- Dougherty E.R., Astola J. (1993) Mathematical Non-Linear Image Processing. Kluwer Academic Publishers, London.
- Drzymała J. (2001) Podstawy mineralurgii. Oficyna Wydawnicza Politechniki Wrocławskiej, Wrocław, Poland (in Polish).
- Dutkiewicz E.T. (1998) Fizykochemia powierzchni. WNT, Warsaw, Poland (in Polish).
- Egry I., Lohofer G., Neuhaus P., Sauerland S. (1992) Surface Tension Measurements of Liquid Metals Using Levitation, Microgravity, and Image Processing. Int. Journal of Thermophysics, Vol. 13, No. 1, pp. 65-74.
- Emelyanenko A.M. (2004) The Application of Digital Image Processing to Study Surface Phenomena. Progress in Colloid and Polymer Science, Vol. 128, pp. 199-201.
- Emelyanenko A.M., Boinovich L.B. (2001) The Role of Discretization in Video Image Processing of Sessile and Pendant Drop Profiles. Colloids and Surfaces A: Physicochemical and Engineering Aspects, Vol. 189, pp. 197-202.
- Eng H.L., Ma K.K. (2001) Noise Adaptive Soft-Switching Median Filter. IEEE Transactions on Image Processing, Vol. 10, No. 2, pp. 242-251.
- Erhardt-Ferron A. (2000) Theory and Applications of Digital Image Processing. University of Applied Sciences, Offenburg.
- Eustathopoulos N., Nicholas M.G., Drevet B. (eds.) (1999) Wettability at High Temperatures. Pergamon.
- Fabijańska A. (2012) Nowoczesne metody segmentacji obrazów w wybranych przemysłowych i medycznych systemach wizyjnych. Wydawnictwo Politechniki Łódzkiej, Łódź (in Polish).
- Fabijańska A. (2007). Algorytmy poprawy jakości obrazów w wysokotemperaturowych pomiarach właściwości fizykochemicznych wybranych metali i ich stopów. PhD Thesis, Lodz University of Technology, Łódź, Poland (in Polish).
- Fabijańska A., Sankowski D. (2007) Image Noise Removal. The New Approach. IEEE 9th International Conference: The Experience of Designing and Application of CAD Systems in Microelectronic CADSM, Lviv-Polyana, Ukraine, pp. 457-459.
- Fabijańska A., Sankowski D. (2011) Noise Adaptive Switching Median-Based Filter for Impulse Noise Removal from Extremely-Corrupted Images. IET Image Processing, Vol. 5, No. 5, pp. 472-480.

- Forsyth D.A., Ponce J. (2003) *Computer Vision. A Modern Approach*. Prentice Hall, New Jersey.
- Fu K.S., Mui J.K. (1981) A Survey on Image Segmentation, *Pattern Recognition Letters*, Vol. 13, No. 1, pp. 3-16.
- Gamma E., Helm R., Johnson R., Vlissides J. (1995) *Design Patterns: Elements of Reusable Object-Oriented Software*. Addison-Wesley, Massachusetts.
- Garnett R., Huegerich T., Chui C., He W.J. (2005) A Universal Noise Removal Algorithm with an Impulse Detector. *IEEE Transactions on Image Processing*, Vol. 14, No. 11, pp. 1747-1754.
- Gil J., Werman M. (1993) Computing 2-D Min, Median, and Max Filters. *IEEE Transactions on Pattern Analysis and Machine Intelligence*, Vol. 15, No. 5, pp. 504-507.
- Girault H., Schiffrin D.J., Smith B.J. (1984) The Measurement of Interfacial Tension of Pendant Drops Using a Video Image Profile Digitizer. *Journal of Colloid and Interface Science*, Vol. 101, pp. 257-266.
- Gonzalez R.C., Wintz P. (1987) *Digital Image Processing*. Addison-Wesley Publishing, Reading.
- Gonzalez R.C., Woods R.E. (2007) *Digital Image Processing*. Prentice Hall, New Jersey.
- Guangjin Z., Jiegu L. (1997) Some Problems of 2D Morphological and Median Filters. *Journal of Shanghai University (English Edition)*, Vol. 1, No. 3, pp. 245-248.
- Hader D.P. (2000) *Image Analysis: Methods and Applications*. CRC Press.
- Hamza A.B., Luque-Escamilla P.L., Martinez-Aroza J., Roman-Roldan R. (1999) Removing Noise and Preserving Details with Relaxed Median Filters. *Journal of Mathematical Imaging and Vision*, Vol. 11, No. 2, pp. 161-177.
- Hansen F.K. (1993) Surface Tension by Image Analysis: Fast and Automatic Measurements of Pendant and Sessile Drops and Bubbles. *Journal of Colloid and Interface Science*, Vol. 160, pp. 209-217.
- Hansen F.K., Rodsrud G. (1991) Surface Tension by Pendant Drop. *Journal of Colloid and Interface Science*, Vol. 141, pp. 1-9.
- Haralick R.M. (1982) Zero Crossing of Second Directional Derivative Edge Operator. *SPIE Symposium on Robot Vision*, 336, Washington, pp. 91-99.

- Haralick R.M., Shapiro L.G. (1985) Survey: Image Segmentation Techniques. *Computer Vision, Graphics, and Image Processing*, Vol. 29, pp. 100-132.
- Hartland S. (ed.) (2004) *Surface and Interfacial Tension: Measurement, Theory, and Applications*. CRC Press.
- Howell S.B. (2006) *Handbook of CCD Astronomy*, Cambridge University Press, Cambridge.
- Huang T.S. (1981) *Two-Dimensional Signal Processing II: Transforms and Median Filters*. Springer.
- Huh C., Reed R.L. (1983) A Method for Estimating Interfacial Tensions and Contacts Angles from Sessile and Pendant Drop Shapes. *Journal of Colloid and Interface Science*, Vol. 9, pp. 1472-1484.
- Hung M.C., Ridd M. (2002) A Subpixel Classifier for Urban Land-Cover Mapping Based on a Maximum-Likelihood Approach and Expert System Rules. *Photogrammetric, Engineering & Remote Sensing*, Vol. 68, pp. 1173-1180.
- Ibach H. (2007) *Physics of Surfaces and Interfaces*. Springer.
- Jahne B. (2002) *Digital Image Processing*. Springer, Berlin, Heidelberg, New York.
- Jahne B. (2004) *Practical Handbook on Image Processing for Scientific and Technical Applications*. CRC Press.
- Jain A.K. (1989) *Fundamentals of Digital Image Processing*. Prentice Hall, New Jersey.
- Jensen J.R. (2004) *Introductory Digital Image Processing*. Prentice Hall, New Jersey.
- Jeżewski S. (2006) Model oświetlenia wysokotemperaturowego w zagadnieniach przetwarzania obrazu próbek na granicy fazy stałej i ciekłej. PhD Thesis. AGH University of Science and Technology, Cracow, Poland (in Polish).
- Jivin I., Rotman S.R. (2008) Edge Impact on Subpixel Target Detection in Hyperspectral Imagery. *Proceedings IEEE 25th Convention of Electrical and Electronics Engineers*, pp. 100-104.
- Kernco Instruments (1999) VCA 2000 Video Contact Angle Meter. Mat. Kernco Instruments Co. Inc., El Paso.
- Kinloch A.J. (1980) Review: The Science of Adhesion. *Journal on Material Science*, Vol. 15, pp. 2141-2166.

- Koszmider T. (2009) Zintegrowany system komputerowy do pomiaru cech geometrycznych próbek metali i ich stopów znajdujących się w wysokich temperaturach. PhD Thesis, Lodz University of Technology, Lodz, Poland (in Polish).
- Koszmider T., Strzecha K. (2008) New Segmentation Algorithms of Metal's Drop Images from THERMO-WET System. Proc. Iv IEEE Int. Conf. Memstech'2008, Polyana-Lviv, pp. 81-83.
- Kravchonok A.I., Zalesky B.A., Lukashevich P.V. (2007) An Algorithm for Median Filtering on the Basis of Merging of Ordered Columns. Pattern Recognition and Image Analysis, Vol. 17, No. 3, pp. 402-407.
- Kwok D.Y., Neumann A.W. (2000) Contact Angle Interpretation in Terms of Solid Surface Tension. Colloid Surfaces A: Physicochemical and Engineering Aspects, Vol. 161, pp. 31-48.
- Lam C.N.C, Lu J.Y., Neumann A.W. (2001a) Measuring Contact Angle. [in]: Holmberg K., Schwuger M.J., Shsh D.O. (eds.) Handbook of Applied Surface and Colloid Chemistry. Part 5: Analysis and Characterization in Surface Chemistry. Willey Europe.
- Lam C.N.C., Ko R.H.Y., Li D., Hair M.L., Neuman A.W. (2001b) Dynamic Cycling Contact Angle Measurements: Study of Advancing and Receding Contact Angles. Journal of Colloid and Interface Science, Vol. 243, No. 11, pp. 208-218.
- Lee C., Guo S., Hsu C. (2004) A Novel Fuzzy Filter for Impulse Noise Removal. Advances in Neural Networks ISNN 2004, Lecture Notes in Computer Science, Vol. 3174, pp. 375-380.
- Lee Y., Takahashi N., Tsai D., Ishii K. (2007) Adaptive Partial Median Filter for Early CT Signs of Acute Cerebral Infarction. International Journal of Computer Assisted Radiology and Surgery, Vol. 2, No. 2, pp. 105-115.
- Li J., Gray R.M. (2000) Image Segmentation and Compression Using Hidden Markov Models. Springer-Verlag, Berlin.
- Lim J.S. (1990) Two-Dimensional Signal and Image Processing. Prentice Hall, New Jersey.
- Marr D., Hildreth E. (1980) Theory of Edge Detection. Proceedings of Royal Society, B-207, pp. 187-217.
- Materka A. (1991) Elementy cyfrowego przetwarzania i analizy obrazów. PWN, Warsaw (in Polish).

- Matsunawa A., Ohji T. (1982) Role of Surface Tension in Fusion Welding, Part I. Transactions of Japan Welding Research Institute, Vol. 11, pp. 145-154.
- Matsunawa A., Ohji T. (1983) Role of Surface Tension in Fusion Welding, Part II. Transactions of Japan Welding Research Institute, Vol. 12, pp. 123-130.
- Matsunawa A., Ohji T. (1984) Role of Surface Tension in Fusion Welding, Part III. Transactions of Japan Welding Research Institute, Vol. 13, pp. 147-156.
- Metcalf A.G. (1981) Interfaces in Metal-Matrix Composites. Academic Press, New York.
- Missal W. (1974) Energia powierzchni rozdziału faz w metalach. Wydawnictwo Śląsk, Katowice (in Polish).
- Mittal K.L. (2006) Contact Angle, Wettability and Adhesion. VSP.
- Morillas S., Gregori V., Peris-Fajarnés G., Latorre P. (2005) A New Vector Median Filter Based on Fuzzy Metrics. Image Analysis and Recognition, Lecture Notes in Computer Science, Vol. 3656, pp. 81-90.
- Mortensen A. (1991) Interfacial Phenomena in the Solidification Processing of Metal-Matrix Composites. Material Science and Engineering Vol. A-135, pp. 1-11.
- Murr L.E. (1975) Interfacial Phenomena in Metals And Alloys. Addison-Wesley Publishing, Reading.
- Myers D. (1999) Surfaces, Interfaces, and Colloids: Principles and Applications. Wiley-VCH.
- Nakamura J. (2005) Image Sensors and Signal Processing for Digital Still Cameras. CRC Press.
- Ng P.E., Ma K.K. (2006) A Switching Median Filter with Boundary Discriminative Noise Detection for Extremely Corrupted Images. IEEE Transactions on Image Processing, Vol. 15, No. 6, pp. 1506-1516.
- Nicholas M.G. (ed.) (1990) Joining of Ceramics. Chapman & Hall, London.
- Nieniewski M. (2005) Segmentacja obrazów cyfrowych. Metody segmentacji wododziałowej. Akademicka Oficyna Wydawnicza Exit, Warsaw (in Polish).
- Nikolaidis N., Pitas I. (2001) 3d Image Processing Algorithms. Wiley-Interscience.
- Pallas N.R., Harrison Y.R. (1990) An Automated Drop Shape Apparatus and the Surface Tension of Pure Water. Colloids Surfaces, Vol. 43, pp. 169-194.
- Pask J., Evans A. (eds.) (1981) Surfaces and Interfaces in Ceramic and Ceramic-Metal Systems. Plenum Publishing Co., New York.

- Pavlidis T. (1987) Grafika i przetwarzanie obrazów. WNT, Warsaw (in Polish).
- Pitas I. (2001) Digital Image Processing Algorithms and Applications. Wiley-Interscience.
- Pitas I., Venetsanopou, A. (1990) Nonlinear Digital Filters: Principles and Application. Springer.
- Popel S.I. (2003) Surface Phenomena in Melts. Cambridge International Science Publishing.
- Pratt W.K. (2007) Digital Image Processing. John Wiley & Sons.
- Reed T.R., Du Buf J.M.H. (1993) A Review of Recent Texture Segmentation and Feature Extraction Techniques. Computer Vision, Graphics and Image Processing, Vol. 57, pp. 359-372.
- Rosen M.J. (2004) Surfactants and Interfacial Phenomena. Wiley-Interscience, Los Altos.
- Rotenberg Y., Boruvka L., Neumann A.W. (1983) Determination of Surface Tension and Contact Angle from the shapes of Axisymmetric Fluid Interfaces. Journal of Colloid and Interface Science, Vol. 93, pp. 169-183.
- Russ J.C. (2002) The Image Processing Handbook. CRC Press.
- Safran S.A. (2003) Statistical Thermodynamics of Surfaces, Interfaces, and Membranes. Westview Press.
- Sankowski D., Mosorow W., Strzecha, K. (2011) Przetwarzanie i analiza obrazów w systemach przemysłowych. Wybrane zastosowania. PWN, Warsaw (in Polish).
- Sankowski D., Senkara J., Strzecha K., Jeżewski S. (2001a) Automatic Investigation of Surface Phenomena in High Temperature Solid and Liquid Contacts. 18th IEEE Instrumentation and Measurement Technology Conference, Budapest, pp. 346-249.
- Sankowski D., Senkara J., Strzecha K., Jeżewski S. (2001b) Image Segmentation Algorithms in High Temperature Measurements of Physical Properties Using CCD Camera. Proc. 18th IEEE Instrumentation and Measurement Technology Conf., Budapest, pp. 346-249.
- Sankowski D., Strzecha K., Janicki M., Koszmider T. (2006) THERMO-WET: Case Study of Control Application Design. Selected Problems of Computer Science, Warsaw, pp. 392-401.

- Sankowski D., Strzecha K., Jeżewski S. (2000a) Image Processing in Physical Parameters Measurement. Proc. 16th Imeko World Congress, Vienna, pp. 277-283.
- Sankowski D., Strzecha K., Jeżewski S. (2000b) Digital Image Analysis in Measurement of Surface Tension and Wettability Angle. Proc. IEEE Int. Conf. on Modern Problems in Telecommunication, Computer Science and Engineers Training, Lviv, pp. 129-130.
- Sankowski D., Strzecha K., Jeżewski S., Senkara J., Łobodziński W. (1999) Computerised Device With CCD Camera for Measurement of Surface Tension and Wetting Angle in Solid-Liquid Systems. Proc. IEEE Instrumentation and Measurement Technology Conf., Venice, pp. 164-168.
- Schulte S., de Witte V., Nachttegael M., van der Weken D., Kerre E.E. (2005) A New Fuzzy Multi-channel Filter for the Reduction of Impulse Noise. Pattern Recognition and Image Analysis, Lecture Notes in Computer Science, Vol. 3522, pp. 368-375.
- Senkara J., Windyga A. (1990) Podstawy teorii procesów spajania. Wydawnictwo Politechniki Warszawskiej, Warsaw (in Polish).
- Senthilkumaran N., Rajesh R. (2009) Edge Detection Techniques for Image Segmentation – A Survey of Soft Computing Approaches. International Journal of Recent Trends in Engineering, Vol. 1, No. 2, pp. 250-254.
- Shapiro L., Rosenfeld A. (1992) Computer Vision and Image Processing. Academic Press, Boston.
- Shapiro L., Stockman G. (2000) Computer Vision. Prentice Hall, New Jersey.
- Sharma G. (2002) Digital Color Imaging Handbook. CRC Press.
- Smolka B. (2007) Peer Group Vector Median Filter. Pattern Recognition, Lecture Notes in Computer Science, Vol. 4713, pp. 314-323.
- Smolka B., Szczepanski M., Plataniotis K.N., Venetsanopoulos A.N. (2001) Fast Modified Vector Median Filter. Computer Analysis of Images and Patterns: 9th International Conference, CAIP, Warsaw, Poland, September 5-7, 2001, Proceedings, Lecture Notes in Computer Science, Vol. 2124, p. 570.
- Song B., Springer J. (1996) Determination of Interfacial Tension from the Profile of a Pendant Drop Using Computer-Aided Image Processing: 2. Experimental. Journal of Colloid and Interface Science, Vol. 184, No 1, pp. 77-91.

- Sonka M., Hlavac V., Boyle R. (2007) *Image Processing, Analysis, and Machine Vision*. Thomson-Engineering.
- Staldera A.F., Melchiorb T., Müllerb M., Saged D., Bluc T., Unserd M. (2010) Low-Bond Axisymmetric Drop Shape Analysis for Surface Tension and Contact Angle Measurements of Sessile Drops. *Colloids and Surfaces A: Physicochemical and Engineering Aspects*, Vol. 364, pp. 72-81.
- Strzecha K. (2002) *Zastosowanie przetwarzania i analizy obrazów w wysokotemperaturowych pomiarach własności fizykochemicznych wybranych materiałów*. PhD Thesis, Lodz University of Technology, Lodz, Poland (in Polish).
- Strzecha K., Bąkała M., Fabijańska A., Koszmider T. (2010) New Ideas in High Temperature Computerized Measurements of Surface Properties. *Proc. 6th Int. Conf. Perspective Technologies and Methods in Mems Design*. Lviv-Polyana, pp. 81-84.
- Strzecha K., Koszmider T. (2008) Drop Shape Analysis for Measurements of Surface Tension and Wetting Angle of Metals at High Temperatures. *Proc. IV IEEE Int. Conf. Memstech'2008, Polyana-Lviv*, pp. 57-59.
- Strzecha K., Koszmider T., Zarębski D., Łobodziński W. (2012) Passive Auto-Focus Algorithm for Correcting Image Distorsions Caused by Gas Flow in High-Temperature Measurements of Surface Phenomena. *Image Processing & Communications*, Vol. 17, No. 4, pp. 379-384.
- Strzecha K., Sankowski D., Janicki M., Koszmider T. (2006) Control Application Design of THERMO-WET System. *Proc. VIII Imeko World Congress, Rio De Janeiro*.
- Sun J. (2006) *Edge Detection, Image Segmentation and Their Applications in Microarray Image Analysis*. Proquest/UMI.
- Sun T., Neuvo Y. (1994) Detail-Preserving Median Based Filters in Image Processing. *Pattern Recognition Letters*, Vol. 15, pp. 341-347.
- Suri J.S., Setarehdan S.K, Singh S. (eds) (2002) *Advanced Algorithmic Approaches to Medical Image Segmentation: State of the Art Applications in Cardiology, Neurology, Mammography and Pathology*. Springer-Verlag, Berlin.
- Suri J.S., Wilson D., Laxminaryan, S. (2005) *Handbook of Biomedical Image Analysis: Volume 1: Segmentation Models*, Springer.

- Tadeusiewicz R., Korohoda P. (1997) *Computer Analysis and Image Processing. Progress of Telecommunication Foundation Publishing House, Kraków.*
- Tadeusiewicz R., Śmietański J. (2011) *Acquisition of Medical Images and their Processing, Analysis, Automatic Recognition and Diagnostic Interpretation. Wydawnictwo STN, Kraków.*
- Teuber J. (1993) *Digital Image Processing. Prentice Hall, New Jersey.*
- Toprak A., Guler I. (2006) *Suppression of Impulse Noise in Medical Images with the Use of Fuzzy Adaptive Median Filter. Journal of Medical Systems, Vol. 30, No. 6, pp. 465-471.*
- Trakhtenberg L.I., Lin S.H., Ilegbusi O.J. (eds.) (2007) *Physico-Chemical Phenomena in Thin Films and at Solid Surfaces. Academic Press.*
- Umbaugh S.E. (2005) *Computer Imaging: Digital Image Analysis And Processing. CRC Press.*
- Venables J.A. (2006) *Introduction to Surface and Thin Film Processes. Cambridge University Press.*
- Watkins C.D., Sadun A., Marenka S. (1995) *Nowoczesne metody przetwarzania obrazu. WNT, Warsaw (in Polish).*
- Welk M., Feddern C., Burgeth B., Weickert J. (2003) *Median Filtering of Tensor-Valued Images. Pattern Recognition, Lecture Notes in Computer Science, Vol. 2781, pp. 17-24.*
- Welk M., Becker F., Schnörr C., Weickert J. (2005) *Matrix-Valued Filters As Convex Programs. Scale Space and PDE Methods in Computer Vision, Lecture Notes in Computer Science, Vol. 3459, pp. 204-216.*
- Weng Q.H., Lu D.S. (2009) *Landscape As a Continuum: An Examination of the Urban Landscape Structures and Dynamics of Indianapolis City, 1991–2000, by Using Satellite Images. International Journal of Remote Sensing, Vol. 30, pp. 2547-2577.*
- Wiatr K. (2002) *Sprzętowe implementacje algorytmów przetwarzania obrazów w systemach wizyjnych czasu rzeczywistego. Uczelniane Wydawnictwa Naukowo-Dydaktyczne AGH, Kraków.*
- Wiatr K. (2003) *Akceleracja obliczeń w systemach wizyjnych. WNT, Warszawa.*
- Wirth M., Nikitenko D. (2005) *Suppression of Stripe Artifacts in Mammograms Using Weighted Median Filtering. Image Analysis and Recognition, Lecture Notes in Computer Science, Vol. 3656, pp. 966-973.*

- Woodruff D.P. (1973) *The Solid-Liquid Interface*. Cambridge University Press.
- Woods J.W. (2006) *Multidimensional Signal, Image, and Video Processing and Coding*. Academic Press Inc. Orlando.
- Woodward R.P. (ed.) (1996) *Two Dimensional Contact Angle and Surface Tension Mapping*. First Ten Angstroms, Portsmouth.
- Woźnicki J. (1996) *Podstawowe techniki przetwarzania obrazu*. WKŁ, Warsaw, Poland (in Polish).
- Wu C.H., Homg S.J. (2003) Fast and Scalable Selection Algorithms with Applications to Median Filtering. *IEEE Transactions on Parallel and Distributed Systems*, Vol. 14, No. 10, pp. 983-992.
- Xu Z., Masliyah J.H. (2002) Contact Angle Measurement on Oxide and Related Surfaces. in: Hubbar, D.A., (ed.) *Encyclopedia Of Surface and Colloid Science*. Marcel Dekker, New York, pp. 1228-1241.
- Yin L, Yang R., Gabbouj M., Neuvo Y. (1996) Weighted Median Filters: A Tutorial. *IEEE Transactions on Circuits and Systems*, Vol. 43, No. 3, pp. 157-192.
- Yoo T.S. (ed.) (2004) *Insight into Images: Principles and Practice for Segmentation, Registration, and Image Analysis*, AK Peters.
- Young T., Gerbrands J.J., Van Vliet L.J. (1998) *Fundamentals of Image Processing*. The Delft University Of Technology, Delft.
- Zangwill A. (1988) *Physics at Surfaces*. Cambridge University Press.
- Zhang Y.J. (ed.) (2006) *Advances in Image and Video Segmentation*. IRMPress.
- Ziou D., Tabbone S. (1998) Edge Detection Techniques – An Overview. *International Journal of Pattern Recognition and Image Analysis*, Vol. 8, pp. 537-559.
- Zuech N. (2000) *Understanding and Applying Computer Vision*. Marcel Dekker Inc., New York.
- Zuo Y.Y., Do C., Neumann A.W. (2007) Automatic Measurement of Surface Tension from Noisy Images Using a Component Labeling Method. *Colloids and Surfaces A: Physicochemical and Engineering Aspects*, Vol. 299, pp. 109-116.

List of the Selected Symbols and Abbreviations

- V_i – speed of light in medium i
- ∇L – gradient image
- \oplus – convolution
- ADSA – Axisymmetric Drop Shape Analysis
- CCD – Charge Coupled Device
- JDBC – Java Database Connectivity
- MSE – Mean Squared Error
- PID – Proportional-Integral-Derivative
- SNR – Signal-to-Noise Ratio
- SQL – Structured Query Language
- XML – Extensible Markup Language
- $L(x, y)$ – digital image
- T – temperature
- $d(x, y)$ – map of disturbed pixels in the digital image
- g – gravitational acceleration
- n – light refraction in gas
- α – capillary constant
- γ – density of gas
- θ – wetting angle
- $\mu(x, y)$ – mean value of brightness of the local area in the digital image
- ρ – density
- σ – surface tension
- $\sigma(x, y)$ – standard deviation of brightness of the local area in the digital image

List of Figures

Fig. 2.1. Sessile drop (measured parameters indicated).....	11
Fig. 2.2. The conditions of the thermodynamic equilibrium	13
Fig. 3.1. The main view of computerized device for the automated measurement of the surface tension and the wetting angle 1– the heating chamber of the furnace; 2 - the temperature controllers; 3 – the system of technological gas supply; 4- the specimen insertion mechanism; 5 – the vision subsystem including CCD camera and infrared filters changer; 6–the computer controlling measurement process and processing measurement data.....	14
Fig. 3.2. Block diagram of the automated measurement system	16
Fig. 3.3. THERMO-WET system’s module dependencies.....	19
Fig. 3.4. The CommDevice class representing the logical communication device	20
Fig. 3.5. The CommLibrary class realizing the physical implementation of the communication functionality.....	21
Fig. 3.6. The CommProtocolFactory class incorporating single-character transmission modes	22
Fig. 3.7. The FrameLayerProtocolFactory class incorporating frame-level character bundle formatting standards	21
Fig. 3.8. The SerialCommDevice inheriting from the abstract class representing the logical communication device driver.....	23
Fig. 3.9. Task Experiment Scheduler functionality.....	24
Fig. 4.1. Instrumental background elimination; a) original image, copper, 817°C; b) master dark – after histogram stretching; c) corrected image	26
Fig. 4.2. Flow diagram of master dark frame construction algorithm.....	27
Fig. 4.3. Compensation of pixel non uniform sensitivity; a) original image, copper, 10940C; b) image after correction; 1) image before segmentation; 2) image after segmentation.....	28
Fig. 4.4. Influence of optical filter selection on image quality; a) original image, palladium, 1564°C; b) and c) improper filter selection; d) proper filter selection.....	30
Fig. 4.5. Change of image contrast in function of temperature. Images obtained without filter (FILTER 0) are considered	31

Fig. 4.6. Change of image contrast as a function of temperature for all filters from THERMO-WET vision unit.....	30
Fig. 4.7. Block diagram of algorithm of optical filters automatic change.....	33
Fig. 4.8. Block diagram of algorithm of contrast maximum crossing detection	34
Fig. 4.9. Uncorrupted test images used in the tests of proposed filtration algorithm.....	38
Fig. 4.10. Test images corrupted by Gaussian noise.....	39
Fig. 4.11. Test images corrupted by salt-and-pepper noise	39
Fig. 4.12. Comparison of restoration results for test images corrupted by Gaussian noise of deviation equal to 15	43
Fig. 4.13. Comparison of restoration results for test images corrupted by salt-and-pepper noise of level 30%	44
Fig. 5.1. Presumed distribution of isotherms in the gas laminar flowing through the heating chamber of the furnace (Strzecha et al., 2012) .	47
Fig. 5.2. The phenomenon of aura around a specimen and the surface of the measurement table	48
Fig. 5.3. The transition of light rays through the borders of two media with different temperatures (Strzecha et al., 2012)	49
Fig. 5.4. The mesh of horizontal oriented auto-focus points.....	50
Fig. 5.5. The result of the second stage of auto-focus algorithm for the mesh of horizontal auto-focus points	51
Fig. 5.6. Contrast ratio as a function of distance of the camera from the specimen: A - minimum distance, B - optimal contrast, C - maximum distance	51
Fig. 5.7. Images obtained during the experimental verification of auto-focus algorithm: A - minimum distance, B - optimal contrast, C - maximum distance	52
Fig. 5.8. Contrast ratio as a function of distance of the camera from a specimen for two different values of gradient threshold.....	52
Fig. 5.9. Contrast ratio as a function of distance of the camera from a specimen for two different methods of determining the value of the gradient.....	53
Fig. 5.10. Contrast ratio as a function of distance of the camera from a specimen with and without averaging.....	53
Fig. 5.11. Block diagram of aura extraction algorithm.....	54

Fig. 5.12. Influence of aura removal process on image segmentation quality; a) original image, copper, 1239°C; b) original image after segmentation; c) aura-removed image after segmentation.....	56
Fig. 6.1. Specimen location points.....	58
Fig. 6.2. Idea of fast drop localization algorithm.....	58
Fig. 6.3. Sobel mask for four basic directions of the vector gradient.....	60
Fig. 6.4. The use of gradient filter masks in different drop areas	59
Fig. 6.5. Fig. 6.5. Point and n-neighbor detection masks	60
Fig. 6.6. The final result of the segmentation process.....	62
Fig. 6.7. The deformation of the specimen profile at the contact point of the three phases.....	63
Fig. 6.8. Determination of extra points of the specimen profile.....	64
Fig. 6.9. Results of contact angle determination in exemplary image of the low carbon steel specimen at the temperature 1500°C: a) original image; b) results obtained using the original profile; c) results obtained after extending the specimen profile using the presented method.....	65
Fig. 6.10. Results of contact angle determination between Al ₂ O ₃ and copper at temperature 1050°C-1600°C	66
Fig. 6.11. Successive steps of coarse edge determination; (a) exemplary image of steel cylinder at 1020°C; (b) horizontal gradient; (c) vertical gradient; (d) coarse vertical edge; (e) coarse horizontal edge; (f) complete coarse edge composed from horizontal and vertical component.....	69
Fig. 6.12. The idea of sub-pixel edge detection using the proposed method ...	69
Fig. 6.13. Results of edge detection with the sub-pixel accuracy; (a) original image; (b) edge detected with pixel accuracy; (c) sub-pixel edge; 1 – low carbon steel, 1200°C; 2 – low carbon steel I, 1000°C; 3 – silver, 1200°C; 4 – low carbon steel, 880°C	70

List of Tables

Table 4.1. Images corresponding with points marked on curve from Fig. 4.5 ..	32
Table 4.2. Gaussian noise removal results	41
Table 4.3. Salt-and-pepper noise removal results.....	42

ISBN 978-83-7283-742-4